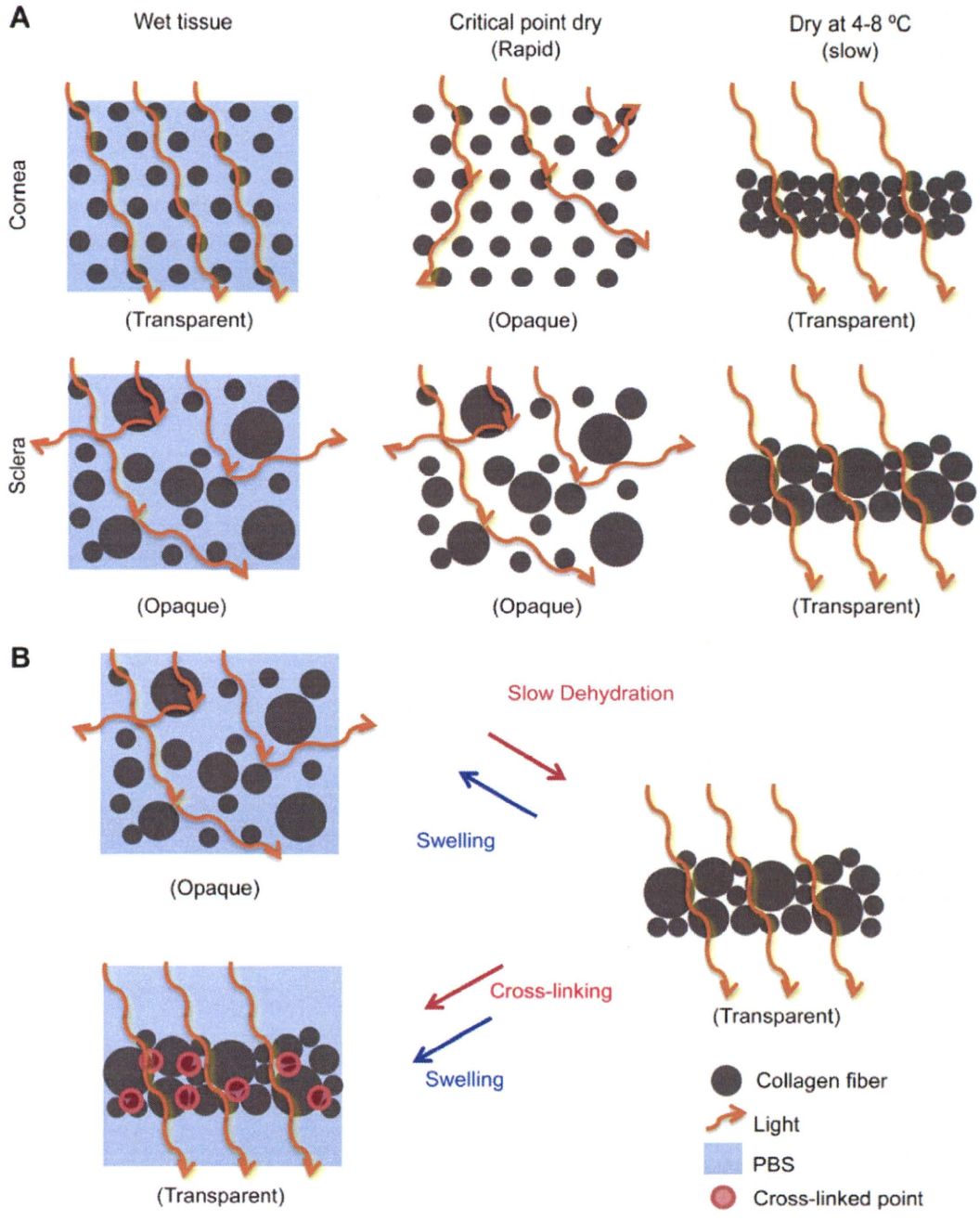

Fig. 9. Schematic illustration of structural effect on the transparency of cornea and sclera which were treated by low temperature dry or critical point dry (A), and collagen structure during the stabilization of transparency by chemical cross-linking (B).

and C). Small fiber-like structures (1–3 mm length), which connected cells and the surface of optically cleared sclera, were observed on the cross-section of the interface on the high-magnification imaging by SEM (Fig. 8D). Furthermore, microvilli were also observed on the surface of the cultured cells (Fig. 8E).

4. Discussion

Schematic illustrations of the proposed relationship between light transmission and structure in cornea and sclera, which were treated by two different dry processes, were given in Fig 9. Generally, the uniformity of fiber diameter and regularity of inter-fiber distance are considered to be essential for the regulation of visible-light transmission in cornea and sclera *in vivo* (the left column, Fig. 9A). Critical point drying is commonly used for dehydrating tissues with preserving their structures at wet condition, but treated cornea quickly lost its transparency (the first row and the middle column, Fig. 9A), because a stronger irregular light reflection occurs on the surface of collagen fibers in the tissues, which caused by large difference in refractive index between collagen (n = 1.416) [7,18] and air (n = 1.00) than that between collagen and water (n = 1.333) in wet tissue. The high transparency obtained by low-temperature drying treatment (Figs. 1 and 2) may be strongly linked with the reduction of strong light scattering at

collagen–air interface in dense collagen packing (Fig. 3), with accompanying with fiber–fiber connection and inter-fiber space reduction (the right column, Fig. 9A). Such dense fiber packing is thought to be induced by capillary force during slow dehydration at low-temperature [19,20]. Speculations that the relationship between inner fiber packing and transparency are unrelated to the tissue-specific shapes of collagen fiber in cornea and sclera. The speculation is unable to contradict our results that showed that optically cleared cornea and sclera by low-temperature drying had a packed fiber structure that can transmit light (Fig. 1), and the speculation also supported the result of twice increase in transparency of dried rabbit sclera by eliminating irregular light reflection on its surface (Fig. 2).

Based on these results and discussion, the good visible-light transmission of wet chemically cross-linked sclera (Figs. 4 and 5) is caused by cross-linking adjacent fibers, which stabilize their dense fiber packing at wet condition (Figs. 6 and 9B). Repetition of low-temperature drying/chemical cross-linking with EDC/NHS (below 1%/0.5%) also reduced the inter-fiber spaces in the tissue. In addition, the repeated process also drastically reduced the necessary amount of cross-linking reagents for obtaining a high transparency over 50% at 550 nm by more than 90%. The maximum visible-light transmission of wet rabbit sclera obtained by the optimized multi-cycle treatment (Fig. 5) is higher than that of the rabbit sclera dried at low temperature without cover glass (Fig. 2) by 5–10%. This was probably caused by smaller light scattering at water–collagen interface than air–collagen interface on the surface and inside of the tissues with dense fiber packing.

In this study, the multi-cycle optical clearing successfully decreased the visible-light scattering of wet sclera. However, its maximum transparency was unable to be an optical level found in ocular application materials such as transplantable cell carriers [15,16,21–26] and replacement of corneal stroma [27–32]. The drastic reduction of light scattering and light reflection should be achieved for improving their optical property. The specific rigidity (a high Young's module) of this cross-linked sclera (Fig. 7) will provide a good stability in shape and light reflection to transparent tissue. On the other hand, a significant visible-light scattering probably occurs at the untreated rough surface of the wet tissue, and it is the same phenomenon found in dried rabbit sclera treated at low temperature with/without glass cover (Fig. 2). However, cover glass treatment was unsuitable for flatting the surface of wet tissues. Thus, special treatments are expected for obtaining a smooth surface on wet sclera such as excimer laser and micro-keratome treatments, in future study.

Another important function for clinical application is its biocompatibility. This study examined 4 chemical cross-linking reagents (Figs. 4 and 5) and UV irradiation treatment for cross-linking of tissue (Supporting Information 1). Mainly EDC and NHS were used, because they leaves no remain after their cross-linking reagents in their targeted sites. Therefore, no possible toxic substances release into tissues from subsequent cross-link breakdown [21,22,30,31,33,34], or they give no damage to collagen molecules. Observed cell toxicity without quenching reagent for cross-linking reagent caused by the un-reacted activated site and/or adsorbed reagents in the sclera. Arginine was used for quenching the cross-linking reaction and it's for improving cell adhesion [35]. Their efficacy of corneal epithelial cell culturing was successfully conformed. Obtained corneal epithelia cultured on the resultants were multilayered cell membranes with characteristic flat shape like corneal epithelial cells *in vivo* (Fig. 8), and the result indicated the transmission of components from feeder cells through the tissue. However, the thickness of the reconstructed epithelial cell layer was thinner, and the shape of cells on surface was broader than cultivated corneal/oral mucosal epithelium *in vitro* [25,36,37] and cornea *in vivo*. This will be one of our future works that should be studied by examining culture condition, the further modification of treatments of optically cleared sclera, etc.

The irreversibly optically cleared sclera exhibits a potential to use as a cell carrier and replacements for light transmission tissues. Also, our results indicated that the mechanisms of tissue optical clearing and developed method for irreversible optical clearing should be investigated on other tissues for further advance in tissue engineering as well as optical therapies/diagnosis.

5. Conclusion

This study found that dense fiber packing in dried tissue was a key for optical clearing of both cornea and sclera by two structural manipulations through dry processes. In addition, our cycle-treatments with low-temperature drying/chemical cross-linking successfully generate an transparent sclera, which was stable at wet condition. Irreversibly optically cleared sclera also exhibited a strong mechanical property and provided a scaffold character for corneal epithelial regeneration. The new optical clearing processes and the obtained transparent tissues have a potential for using in the field of tissue engineering and medicine, especially for ocular treatments.

Acknowledgements

The authors are grateful to Prof. A. J. Quantock and Mr. T. Duncan of Cardiff University, Dr. K. Fukuyama of Meijigakuin University, and Dr. Y. Hatakeyama of Chiba University for their helpful discussion of structural analysis, and Dr. S. Dong and Miss Y. Sasaki of Tohoku University for their help. This work was financially supported by the Health and Labor Sciences Research Grants of Japan at Tohoku University, and Tohoku University Global COE for conquest of Signal Transduction Disease with "Network Medicine".

Appendix

Figures with essential color discrimination. Figs. 7 and 9 in this article are difficult to interpret in black and white. The full color images can be found in the online version, at doi:10.1016/j.biomaterials.2010.10.002.

Appendix. Supplementary data

Supplementary data associated with this article can be found, in the online version, at doi:10.1016/j.biomaterials.2010.10.002.

References

[1] Moscoso M, Keller JB, Papanicolaou G. Depolarization and blurring of optical images by biological tissue. J Opt Soc Am A Opt Image Sci Vis 2001;18(4):948–60.
[2] Vargas G, Chan EK, Barton JK, Rylander 3rd HG, Welch AJ. Use of an agent to reduce scattering in skin. Lasers Surg Med 1999;24(2):133–41.
[3] Tuchin VV, Maksimova IL, Zimnyakov DA, Kon IL, Mavlutov AH, Mishin AA. Light propagation in tissues with controlled optical properties. J Biomed Opt 1997;2:401–17.
[4] Liu H, Beauvoit B, Kimura M, Chance B. Dependence of tissue optical properties on solute-induced changes in refractive index and osmolarity. J Biomed Opt 1996;1(2):200–11.
[5] Drew C, Milner TE, Rylander CG. Mechanical tissue optical clearing devices: evaluation of enhanced light penetration in skin using optical coherence tomography. J Biomed Opt 2009;14(6):064019.
[6] Rylander CG, Milner TE, Baranov SA, Nelson JS. Mechanical tissue optical clearing devices: enhancement of light penetration in ex vivo porcine skin and adipose tissue. Lasers Surg Med 2008;40(10):688–94.
[7] Doutch J, Quantock AJ, Smith VA, Meek KM. Light transmission in the human cornea as a function of position across the ocular surface: theoretical and experimental aspects. Biophys J 2008;95(11):5092–9.

[8] Meek KM, Fullwood NJ. Corneal and scleral collagens–a microscopist's perspective. Micron 2001;32(3):261–72.
[9] Freund DE, McCally RL, Farrell RA. Direct summation of fields for light scattering by fibrils with applications to normal corneas. Appl Opt 1986;25(16):2739.
[10] Maurice DM. The structure and transparency of the cornea. J Physiol 1957; 136(2):263–86.
[11] Ojeda JL, Ventosa JA, Piedra S. The three-dimensional microanatomy of the rabbit and human cornea. A chemical and mechanical microdissection-SEM approach. J Anat 2001;199(Pt 5):567–76.
[12] Titley KC, Smith DC, Chernecky R, Maric B, Chan A. An SEM examination of etched dentin and the structure of the hybrid layer. J Can Dent Assoc 1995;61 (10):887–94.
[13] Komai Y, Ushiki T. The three-dimensional organization of collagen fibrils in the human cornea and sclera. Invest Ophthalmol Vis Sci 1991;32(8):2244–58.
[14] Takushi E, Asato L, Nakada T. Edible eyeballs from fish. Nature 1990;345:298–9.
[15] Takezawa T, Ozaki K, Takabayashi C. Reconstruction of a hard connective tissue utilizing a pressed silk sheet and type-I collagen as the scaffold for fibroblasts. Tissue Eng 2007;13(6):1357–66.
[16] Takezawa T, Ozaki K, Nitani A, Takabayashi C, Shimo-Oka T. Collagen vitrigel: a novel scaffold that can facilitate a three-dimensional culture for reconstructing organoids. Cell Transplant 2004;13(4):463–73.
[17] Hayashida Y, Nishida K, Yamato M, Yang J, Sugiyama H, Watanabe K, et al. Transplantation of tissue-engineered epithelial cell sheets after excimer laser photoablation reduces postoperative corneal haze. Invest Ophthalmol Vis Sci 2006;47(2):552–7.
[18] Meek KM, Leonard DW, Connon CJ, Dennis S, Khan S. Transparency, swelling and scarring in the corneal stroma. Eye (Lond) 2003;17(8):927–36.
[19] Ciszek JW, Huang L, Tsonchev S, Wang Y, Shull KR, Ratner MA, et al. Assembly of nanorods into designer superstructures: the role of templating, capillary forces, adhesion, and polymer hydration. ACS Nano 2010;4(1):259–66.
[20] Kralchevsky PA, Nagayama K. Capillary interactions between particles bound to interfaces, liquid films and biomembranes. Adv Colloid Interface Sci 2000; 85(2–3):145–92.
[21] Tanaka Y, Kubota A, Matsusaki M, Duncan T, Hatakeyama Y, Fukuyama K, et al. Anisotropic mechanical properties of collagen hydrogels induced by uniaxial-flow for ocular applications. J Biomater Sci Polym Ed; 2010 [Epub ahead of print].
[22] Duncan TJ, Tanaka Y, Shi D, Kubota A, Quantock AJ, Nishida K. Flow-manipulated, crosslinked collagen gels for use as corneal equivalents. Biomaterials 2010;31(34):8996–9005.
[23] Helary C, Bataille I, Abed A, Illoul C, Anglo A, Louedec L, et al. Concentrated collagen hydrogels as dermal substitutes. Biomaterials 2010;31(3):481–90.
[24] Koizumi N, Sakamoto Y, Okumura N, Okahara N, Tsuchiya H, Torii R, et al. Cultivated corneal endothelial cell sheet transplantation in a primate model. Invest Ophthalmol Vis Sci 2007;48(10):4519–26.
[25] Nakamura T, Endo K, Cooper LJ, Fullwood NJ, Tanifuji N, Tsuzuki M, et al. The successful culture and autologous transplantation of rabbit oral mucosal epithelial cells on amniotic membrane. Invest Ophthalmol Vis Sci 2003;44(1): 106–16.
[26] Ng KW, Hutmacher DW. Reduced contraction of skin equivalent engineered using cell sheets cultured in 3D matrices. Biomaterials 2006;27(26): 4591–8.
[27] Carlsson DJ, Li F, Shimmura S, Griffith M. Bioengineered corneas: how close are we? Curr Opin Ophthalmol 2003;14(4):192–7.
[28] Griffith M, Osborne R, Munger R, Xiong X, Doillon CJ, Laycock NL, et al. Functional human corneal equivalents constructed from cell lines. Science 1999;286(5447):2169–72.
[29] Li F, Carlsson D, Lohmann C, Suuronen E, Vascotto S, Kobuch K, et al. Cellular and nerve regeneration within a biosynthetic extracellular matrix for corneal transplantation. Proc Natl Acad Sci U S A 2003;100(26):15346–51.
[30] Liu W, Deng C, McLaughlin CR, Fagerholm P, Lagali NS, Heyne B, et al. Collagen-phosphorylcholine interpenetrating network hydrogels as corneal substitutes. Biomaterials 2009;30(8):1551–9.
[31] Liu Y, Gan L, Carlsson DJ, Fagerholm P, Lagali N, Watsky MA, et al. A simple, cross-linked collagen tissue substitute for corneal implantation. Invest Ophthalmol Vis Sci 2006;47(5):1869–75.
[32] Rafat M, Li F, Fagerholm P, Lagali NS, Watsky MA, Munger R, et al. PEG-stabilized carbodiimide crosslinked collagen–chitosan hydrogels for corneal tissue engineering. Biomaterials 2008;29(29):3960–72.
[33] Marois Y, Chakfe N, Deng X, Marois M, How T, King MW, et al. Carbodiimide cross-linked gelatin: a new coating for porous polyester arterial prostheses. Biomaterials 1995;16(15):1131–9.
[34] Powell HM, Boyce ST. EDC cross-linking improves skin substitute strength and stability. Biomaterials 2006;27(34):5821–7.
[35] Massia SP, Hubbell JA. Immobilized amines and basic amino acids as mimetic heparin-binding domains for cell surface proteoglycan-mediated adhesion. J Biol Chem 1992;267(14):10133–41.
[36] Nishida K, Yamato M, Hayashida Y, Watanabe K, Maeda N, Watanabe H, et al. Functional bioengineered corneal epithelial sheet grafts from corneal stem cells expanded ex vivo on a temperature-responsive cell culture surface. Transplantation 2004;77(3):379–85.
[37] Nishida K, Yamato M, Hayashida Y, Watanabe K, Yamamoto K, Adachi E, et al. Corneal reconstruction with tissue-engineered cell sheets composed of autologous oral mucosal epithelium. N Engl J Med 2004;351(12):1187–96.

Jpn J Ophthalmol 2010;54:494–498
DOI 10.1007/s10384-010-0861-6

LABORATORY INVESTIGATION

Chromosomal Sharing in Atypical Cases of Gelatinous Drop-like Corneal Dystrophy

Motokazu Tsujikawa, Naoyuki Maeda, Kaoru Tsujikawa, Yuichi Hori, Tomoyuki Inoue, and Kohji Nishida

Department of Ophthalmology, Osaka University Graduate School of Medicine, Osaka, Japan

Abstract

Purpose: To present the phenotypic variability both among and within families in Japanese gelatinous drop-like corneal dystrophy (GDLD), and to study the genetic background of the variability.

Methods: Four Japanese families who suffer from bilateral corneal amyloidoses were studied by a molecular genetic method. All families included a patient whose clinical features alone could not be used to diagnose GDLD. In one family, obvious clinical differences were observed between the two members who were patients. Three families had members who suffered from atypical amyloidoses that had not been initially diagnosed as GDLD. For their final diagnoses and for the investigation of the genetic background of these phenotypes, the sequences of the entire *TACSTD2* gene and the genotypes of some polymorphic markers close to the *TACSTD2* gene were studied.

Results: Genetic analysis revealed that all the patients possessed a homozygous Q118X mutation in *TACSTD2*, a major founder mutation in Japanese GDLD. There were no differences in the entire sequence of *TACSTD2* in these patients compared with other GDLD patients. Moreover, the genotyping of polymorphic markers near the *TACSTD2* gene revealed that these patients shared the same founder chromosome as well as the *TACSTD2* gene.

Conclusion: In Japanese GDLD patients, phenotypic variability is observed both among and within families in spite of the allelic homogeneity of Q118X. Even in these atypical cases, the patients shared the same chromosomal region, received from a founder. **Jpn J Ophthalmol** 2010;54:494–498 © Japanese Ophthalmological Society 2010

Keywords: founder effect, GDLD, gelatinous drop-like corneal dystrophy, M1S1, TACSTD2

Introduction

Gelatinous drop-like corneal dystrophy (GDLD; OMIM 204870) is one of the most severe corneal dystrophies with autosomal recessive inheritance. In most cases, its clinical features are grayish corneal amyloid elevation and corneal neovascularization, leading to severe visual impairment.[1,2] We previously identified the gene responsible for GDLD, tumor-associated calcium signal transducer 2 (*TACSTD2*, formerly, *M1S1/TROP2/GA733-1*) using positional cloning.[3,4] Molecular analyses have revealed that most Japanese GDLD patients are homozygous for the Q118X mutation in *TACSTD2*, and 90% of GDLD chromosomes possess this founder mutation.[5–7]

Because of its apparent clinical features, in most cases the diagnosis of GDLD is easy. However, clinical variability and atypical cases have been reported.[8] An important question is whether these atypical cases are caused by genetic background differences, including allelic or locus heterogeneities. In this study, we demonstrated phenotypic variability both among and within families and allelic homogeneity of Q118X among them. Moreover, using intragene and close genetic markers, we showed that even among these atypical cases, a common haplotype is present owing to chromosomal sharing from a common ancestor.

Received: December 7, 2009 / Accepted: March 30, 2010
Correspondence and reprint requests to: Motokazu Tsujikawa, Department of Ophthalmology, Osaka University Graduate School of Medicine, Rm E7, 2-2 Yamadaoka, Suita, Osaka 565-0871, Japan
e-mail: moto@ophthal.med.osaka-u.ac.jp

Patients and Methods

Families and Patients

We studied four Japanese families that included individuals suffering from bilateral corneal amyloid deposition and opacity. In three families, the amyloidoses differed from typical GDLD and the patients could not be diagnosed as GDLD only on the basis of their clinical features and examinations. In the fourth family, one member was diagnosed as having GDLD, not by clinical features but by family history. The final diagnoses of GDLD in these families were obtained by the genetic analyses described here. All patients provided written informed consent for this study and procedures followed the tenets of the Declaration of Helsinki. This study was approved by the institutional review board of the Osaka University Medical School.

Mutation Analysis and Genotyping

From each participant, 20 ml of peripheral blood was taken. Genomic DNA was extracted from white blood cells by standard methods.[9] The entire *TACSTD2* gene region, including the 5′ flanking side was amplified by polymerase chain reaction (PCR) with primers GDLD1F (5′-GAG CAGCTTCCCTGTTCTGA-3′) and GDLD11R (5′-CTG CAGTTTGAAGGAAGTTTCC-3′). PCR was carried out in a 20-μl reaction mixture containing 50 ng of genomic DNA, 10 pmol of each primer, 2.0 mM $MgCl_2$, 1 × reaction buffer (Takara, Tokyo, Japan), 150 μM of each dNTP, and 1.0 U of *ExTaq* polymerase (Takara). Samples were amplified in 32 cycles of 30 s at 94°C, 30 s at 60°C, and 30 s at 72°C. PCR products were purified with a QIAquick PCR purification kit (QIAGEN, Valencia, CA, USA) and then sequenced with a Big-Dye Terminator cycle sequencing kit and analyzed using a 377 automated sequencer (Applied Biosystems, Foster City, CA, USA). To confirm the Q118X mutation detected by sequencing, PCR-restriction fragment length polymorphism analysis (RFLP) was performed. The nucleotide alteration introduces a *Mae*I recognition site, so PCR products obtained with the primer set GDLD3F (5′-ACGTGTCCCACCAACAAGAT-3′) and GDLD3R (5′-AGTTCACGCACCAGCACA-3′) were cleaved with *Mae*I and electrophoresed on 12% polyacrylamide gel.

Genotype analysis was performed on three microsatellite markers, D1S220, D1S2700, and D1S2648 near the *TACSTD2* gene, spanning 400 kbp. One PCR primer for each marker was fluorescently labeled with 6-FAM or HEX (Takara Bio, Shiga, Japan). Each PCR was carried out as described above. PCR products were electrophoresed on 4% denaturing polyacrylamide gels for 2 h and analyzed with the 377 automated sequencer. Genescan analysis software (Applied Biosystems) was used to determine allele size.

Results

Case Reports

Family 1

Family 1 was consanguineous and had two male patients. The proband (II-1) is a typical GDLD patient. He suffered from photophobia, lacrimation, and blurred vision in his first decade. Penetrating keratoplasties were performed on his right eye when he was 22 years old and on his left eye when he was 31 years old, in another hospital. As in some of the other patients, recurrence of amyloid deposition required additional excimer laser phototherapeutic keratectomy in his right eye when he was 46 years old. Even on the transplanted corneas, recurrence of numerous bilateral grayish elevated round depositions and superficial neovascularization can be clearly observed (Fig. 1A).

One of his younger brothers (II-3) was first examined at 39 years of age, when the family members were examined for a segregation study of the *TACSTD2* mutation.[4] The elder brother had had surgical interventions in both eyes by age 30, but the younger brother did not show clear clinical manifestations of GDLD at the same age. He had suffered from photophobia for 2 years; however, he did not have any other symptoms and had not been examined by an ophthalmologist. In the center of the cornea, subepithelial opacity and fine depositions were observed; however, neither an elevated gelatinous region nor neovascularization was observed (Fig. 1B). Late fluorescent staining in both eyes suggested deterioration of the barrier function of the corneal epithelium. He did not need any intervention to his corneal region.

Family 2

Family 2 was also consanguineous and had one male patient, a 9-year-old boy who had mild corneal opacity in both eyes that was diagnosed as macular corneal dystrophy by corneal subspecialists of another university hospital. Small, round white droplets were observed at the subepithelial stroma. The droplets clustered and elevated the epithelium in the center of both corneas; however, similar to patient II-3 in family 1, no prominent elevated region or neovascularization was observed (Fig. 2A). In the center of both corneas, superficial punctuate keratitis and late staining of the epithelium were observed.

Family 3

Family 3 was nonconsanguineous and had one 68-year-old female patient. Clusters of fine yellow lipid droplets were observed beneath the corneal epithelium, mainly in the exposed area from the periphery to the center, and created band-shaped lesions on the scarred corneal stroma. These lipid depositions were different from those of typical GDLD.

Jpn J Ophthalmol
Vol 54: 494–498, 2010

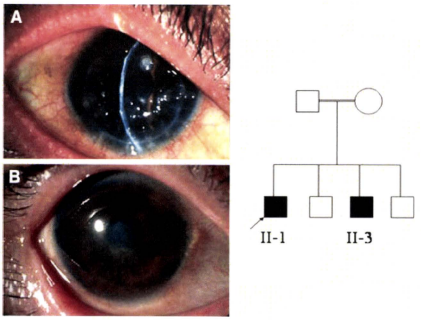

Figure 1A, B. Family 1 shows a phenotypic variability within the family. **A** Right eye of patient II-1 shows typical recurrent gelatinous drop-like corneal dystrophy (GDLD). Best-corrected visual acuity OD was 20/200. **B** Right eye of patient II-3 in family 1. The phenotype is obviously much milder than that of his brother. Best-corrected visual acuity OD was 20/40. Note that there are no elevated gelatinous regions or neovascularization.

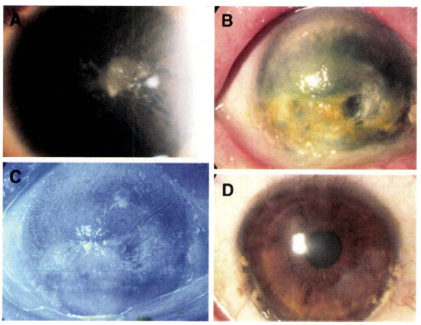

Figure 2A–D. Phenotypic variability among the families. **A** Right eye of the patient in family 2. No prominent elevated regions or neovascularization were observed. Best-corrected visual acuity OD was 20/30. **B** Right eye of the patient in family 3. Note band-shaped yellow fatty deposits and the loss of the palisades of Vogt. Best-corrected visual acuity OD was 20/400. **C** Late fluorescent staining in family 3. **D** Left eye of the patient in family 4. Note band-shaped, lipid-like, yellowish deposition. Best-corrected visual acuity OD was 20/30.

In this case, obvious neovascularization (Fig. 2B) and late fluorescent staining was observed in both eyes (Fig. 2C). On the basis of these clinical examination results, we diagnosed her as having spheroidal corneal degeneration before the genetic analysis.

Family 4

Family 4 is consanguineous and has one 38-year-old male patient who suffered from blurred vision in his first decade. At the corneal facility of another university hospital he was diagnosed with spheroidal corneal degeneration. He underwent lamellar keratoplasty in his left eye at 34 years of age and in his right eye at 36 years. After keratoplasty, the corneal opacity almost completely disappeared except for a subepithelial opacity in the center of the graft. A band-shaped, white deposition in the center of the graft and superficial neovascularization were observed as well (Fig. 2D). Outside the graft, on the peripheral cornea, yellowish deposits that looked like a pinguecula were detected. Late fluorescent staining was also observed in both eyes.

Molecular Genetic Analysis

Sequence and RFLP analysis revealed that all GDLD patients in this study were homozygous for the Q118X mutation (Fig. 3). In families 1 and 2, the Q118X mutation cosegregated with the GDLD phenotype. All of these patients also were homozygous for the D216E polymorphism (data not shown). No other nucleotide alterations were observed, and all sequences from the patients were

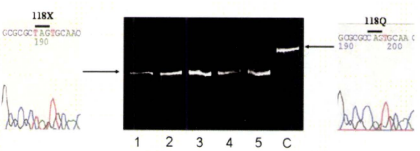

Figure 3. Sequence and restriction fragment length polymorphism analysis of the presented patients. All patients possessed a homozygous Q118X (CAG- > TAG) mutation. *Lanes*: *1*, patient II-1 from family 1; *2*, patient II-3 from family 1; *3*, patient from family 2; *4*, patient from family 3; *5*, patient from family 4; *C*, normal control.

identical. Genotype analysis revealed that all disease chromosomes possessed a 204-bp allele on D1S2752, a 285-bp allele on D1S2648, and a 247-bp allele on D1S220 (Fig. 4). Thus, the haplotype of all disease chromosomes was 204bp-285bp-247bp D1S2752-D1S2648-D1S220).

Discussion

In other corneal dystrophies such as *TGFBI* (formerly βig-h3, transforming growth factor beta-induced gene)-associated inherited corneal dystrophies, apparent genotype–phenotype correlations have been observed.[10–12] For example, granular corneal dystrophy type I is caused mainly by an R555W mutation in *TGFBI*, and Avellino corneal dystrophy by an R124H mutation.[5,11,13] Even varied phenotypes from the same mutation have been reported.[14] We can usually diagnose these dystrophies easily following a clinical

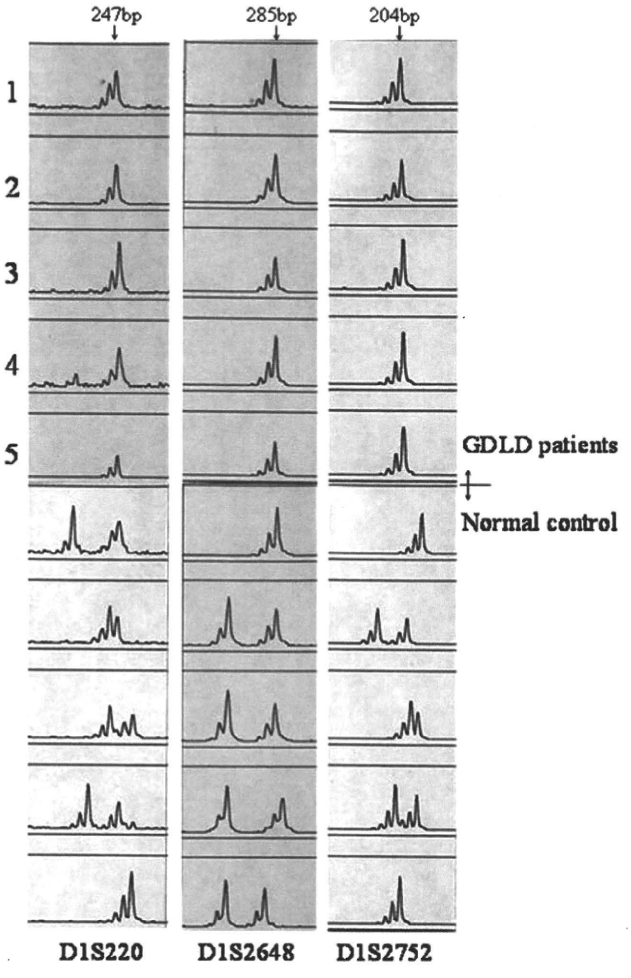

Figure 4. Genotype analysis of the markers flanking the*TACSTD2*. *Top five rows,* analysis results of the GDLD patients: *1*, Patient II-1 from family 1; *2*, patient II-3 from family 1; *3*, patient from family 2; *4*, patient from family 3; *5*, patient from family 4. All patients are homozygotes, and all haplotypes of the disease chromosome were 204bp-285bp-247bp (D1S2752-D1S2648-D1S220). *Bottom five rows,* analysis results of five normal Japanese controls with apparent heterozygosity at these markers.

examination only. In *TGFBI*-associated dystrophies, genetics is the most important factor explaining clinical manifestations.

In typical GDLD patients, bilateral, grayish, elevated round depositions and distinctive severe neovascularization provide enough diagnostic information.[15] However, we and other groups have noticed that there are atypical cases of GDLD that show clinical variability in both age at onset and severity, and in phenotype, even within a family.[8,16]

Family 1 shows clear phenotypic variability within the family. One proband had typical, severe GDLD that required corneal transplantations in both eyes by 31 years of age, whereas his brother had only subepithelial opacification and needed no surgical interventions up to age 39. This brother showed no grayish gelatinous elevation in either eye, and it might have been difficult to diagnose him as having GDLD without a family history. Families 2, 3, and 4 showed phenotypic variability among the families and atypical GDLD.

The cloning of the gene responsible for GDLD enabled us to examine this phenotypic variability on a molecular level. The first question was whether the phenotypic variability was caused by genetic differences within the *TACSTD2* sequence. The phenotypes of GDLD in these patients were quite different; however, the sequence analysis and RFLP results revealed that all patients were homozygous for the Q118X mutation. Therefore, the clinical heterogeneity was clearly not due to allelic or locus heterogeneity. Moreover, the patients showed not only allelic homogeneity, but also shared the same D216E and 204bp-285bp-247bp (D1S2752-D1S2648-D1S220) haplotype, which extends for 400 kb near the *TACSTD2* region. This haplotype is reported to be shared by most typical Japanese GDLD patients,[4,7] indicating that these patients share not only the same disease-causing mutation but also the same chromosomal region, including the same *cis*-acting genetic elements such as the promoter and enhancer. Therefore, we infer that the phenotypic variability among these patients is caused either by *trans*-acting genetic elements or environmental factors.

It is interesting to hypothesize regarding the mechanism of amyloid deposition on the cornea. Corneal amyloidoses occur not only in inherited corneal dystrophies but also as the result of secondary changes after nonspecific chronic disorders and injuries. In these cases, it is usually unilateral, but sometimes it resembles closely the GDLD phenotype. These cases indicate that a genetic factor, such as a *TACSTD2* mutation, is not a prerequisite condition for severe corneal amyloidoses. On the other hand, the amyloid in GDLD has been found to react immunohistochemically with human lactoferrin antibodies and lactoferrin may play a role in amyloid depositions in the cornea.[17,18] The importance of lactoferrin might indicate that several steps may be responsible for amyloid depositions in GDLD, and the malfunctions of *TACSTD2* alone are not enough to account for severe corneal amyloidoses in GDLD. The complex mechanism of amyloid deposition might be one cause of the phenotypic variability presented here. Investigations of factors other than *TACSTD2* malfunctions will lead to better understanding of the mechanism of amyloidoses and more effective therapy without surgical intervention.

We have also reported four other disease-causing mutations in *TACSTD2* (632delA, Q207X, S170X, L186P),[4,19] but we encountered only one homozygous family with each mutation so we could not determine phenotype–genotype correlations among these mutations. However, our impression was that all of those patients had typical GDLD and those among them with the most severe disease possessed the Q207X mutation (data not shown), which translates into a product with a longer carboxyl terminus than the Q118X mutation product. Following those investigations, we now believe that phenotype–genotype correlations may not be involved. The lack of a clear phenotype–genotype correla-

tion indicates that a genetic factor is not an important key to the severity of GDLD, although the dysfunction of *TACSTD2* is necessary for the onset of GDLD. This hypothesis is also supported by the variabilities in the cases we presented.

The phenotypic variability presented here is also important in the diagnosis of GDLD. In families 2, 3, and 4, the patients were not diagnosed with GDLD on the basis of clinical features and examinations. In the family 3 patient, the palisades of Vogt were distinguished and apparent lipid deposition was observed; therefore, we diagnosed him as having typical spheroidal corneal dystrophy. In the patient of family 2, neovascularization, recognized as an important clinical feature of GDLD, was not observed. In such cases, without any significant family history of GDLD, it may be difficult to diagnose the presenting symptoms as GDLD. Thus, these patients were misdiagnosed as having either spheroidal corneal degeneration or macular corneal dystrophy.

On the other hand, late fluorescent staining was observed in all of the patients presented here. That it is an important clinical feature in GDLD diagnosis, and this phenomenon is well explained by the high epithelial permeability observed in GDLD corneas.[20,21] In these atypical cases, the genetic diagnosis presented here in addition to positive late staining of the corneal epithelium is quite useful for diagnosing GDLD, in spite of the possible presence of locus heterogeneity.[22]

Acknowledgments. Drs. Jarema Malicki and Koji Nishiguchi provided many helpful comments on the previous versions of this manuscript. This study was supported by Grants-in-Aid from the Ministry of Education, Culture, Sports, Science and Technology (to M.T.) and by Grants-in-Aid from the Ministry of Health, Labour and Welfare (to M.T.).

References

1. Nakaizumi G. A rare case of corneal dystrophy. Acta Soc Ophthalmol Jpn 1914;18:949–950.
2. Weber FL, Babel J. Gelatinous drop-like dystrophy. A form of primary corneal amyloidosis. Arch Ophthalmol 1980;98:144–148.
3. Tsujikawa M, Kurahashi H, Tanaka T, et al. Homozygosity mapping of a gene responsible for gelatinous drop-like corneal dystrophy to chromosome 1p. Am J Hum Genet 1998;63:1073–1077.
4. Tsujikawa M, Kurahashi H, Tanaka T, et al. Identification of the gene responsible for gelatinous drop-like corneal dystrophy. Nat Genet 1999;21:420–423.
5. Fujiki K, Nakayasu K, Kanai A. Corneal dystrophies in Japan. J Hum Genet 2001;46:431–435.
6. Yamamoto S, Okada M, Tsujikawa M, et al. The spectrum of beta ig-h3 gene mutations in Japanese patients with corneal dystrophy. Cornea 2000;19:S21–23.
7. Tsujikawa M, Tsujikawa K, Maeda N, et al. Rapid detection of M1S1 mutations by the protein truncation test. Invest Ophthalmol Vis Sci 2000;41:2466–2468.
8. Ide T, Nishida K, Maeda N, et al. A spectrum of clinical manifestations of gelatinous drop-like corneal dystrophy in Japan. Am J Ophthalmol 2004;137:1081–1084.
9. Grimberg J, Nawoschik S, Belluscio L, McKee R, Turck A, Eisenberg A. A simple and efficient non-organic procedure for the isolation of genomic DNA from blood. Nucleic Acids Res 1989; 17:8390.
10. Munier FL, Korvatska E, Djemai A, et al. Kerato-epithelin mutations in four 5q31-linked corneal dystrophies. Nat Genet 1997;15: 247–251.
11. Korvatska E, Munier FL, Djemai A, et al. Mutation hot spots in 5q31-linked corneal dystrophies. Am J Hum Genet 1998;62:320–324.
12. Mashima Y, Imamura Y, Konishi M, et al. Homogeneity of kerato-epithelin codon 124 mutations in Japanese patients with either of two types of corneal stromal dystrophy. Am J Hum Genet 1997; 61:1448–1450.
13. Mashima Y, Yamamoto S, Inoue Y, et al. Association of autosomal dominantly inherited corneal dystrophies with BIGH3 gene mutations in Japan. Am J Ophthalmol 2000;130:516–517.
14. Konishi M, Yamada M, Nakamura Y, et al. Varied appearance of cornea of patients with corneal dystrophy associated with R124H Mutation in the BIGH3 gene. Cornea 1999;18:424–429
15. Smolin G. Corneal dystrophies and degenerations. In: Smolin G, Thoft R, editors. Cornea, 3d ed. Boston: Little, Brown; 1994. p. 499–533.
16. Yoshida S, Kumano Y, Numa S, et al. Two brothers with gelatinous drop-like dystrophy at different stage of the disease; role of mutation analysis. Am J Ophthalmol 2002;13:830–832.
17. Klintworth GK, Valnickova Z, Kiclar RA, Baratz KH, Campbell RJ, Enghild JJ. Familial subepithelial corneal amyloidosis—a lactoferrin-related amyloidosis. Invest Ophthalmol Vis Sci 1997; 38:2756–2763.
18. Araki-Sasaki K, Ando Y, Nakamura M, et al. Lactoferrin Glu-561Asp facilitates secondary amyloidosis in the cornea. Br J Ophthalmol 2005;89:684–688.
19. Taniguchi Y, Tsujikawa M, Hibino S, et al. A novel missense mutation in a Japanese patient with gelatinous droplike corneal dystrophy. Am J Ophthalmol 2005;139:186–188.
20. Kinoshita S, Nishida K, Dota A, et al. Epithelial barrier function and ultrastructure of gelatinous drop-like corneal dystrophy. Cornea 2000;19:551–555.
21. Kinoshita S, Adachi W, Sotozono C, et al. Characteristics of the human ocular surface epithelium. Prog Retin Eye Res 2001;20: 639–673.
22. Klintworth GK, Sommer JR, Obrian G, et al. Familial subepithelial corneal amyloidosis (gelatinous drop-like corneal dystrophy): exclusion of linkage to lactoferrin gene. Mol Vis 1998;4:31.

Biomaterials 31 (2010) 8996–9005

Contents lists available at ScienceDirect

Biomaterials

journal homepage: www.elsevier.com/locate/biomaterials

Flow-manipulated, crosslinked collagen gels for use as corneal equivalents

Thomas J. Duncan [a,b,1], Yuji Tanaka [a,c,1], Dong Shi [a,d], Akira Kubota [a], Andrew J. Quantock [b], Kohji Nishida [a,*]

[a] Department of Ophthalmology and Visual Science, School of Medicine, Tohoku University, Sendai, Miyagi 980-8575, Japan
[b] Structural Biophysics Group, School of Optometry and Vision Sciences, Cardiff University, Cardiff CF24 4LU, Wales, United Kingdom
[c] Institute of Advanced Biomedical Engineering and Science, Tokyo Women's Medical University, Shinjuku, Tokyo 162-8666, Japan
[d] Department of Ophthalmology, The Fourth Affiliated Hospital, China Medical University, Shenyang 110005, China

ARTICLE INFO

Article history:
Received 14 July 2010
Accepted 19 August 2010
Available online 9 September 2010

Keywords:
Cornea
Collagen
Crosslinking
TEM (transmission electron microscopy)

ABSTRACT

Our aim was to construct a mechanically stable and optically transparent collagen gel from an acidified atelocollagen solution which is suitable for use as a corneal stromal equivalent. Light transmission and mechanical testing were conducted on variously crosslinked constructs at different pH levels. Ultrastructural analysis was performed to assess directionality of the molecular arrangement produced by flow manipulation, as well as the amount of collagen fibrillogenesis which resulted from different pH and/or crosslinking conditions. Clinical and histological integration of the gels with living tissue was examined following implantation into rabbit corneal intra-stromal pockets. Transmission electron microscopy revealed the importance of the fine control of pH levels during gel formation and indicated that the stage at which collagen fibrillogenesis is halted within the constructs was critically dependent on the pH of the collagen solution. Transparency testing disclosed that high levels of collagen fibrillogenesis, as well as high levels of crosslinker concentration, detrimentally affected the transparency of the construct. As a result, a dual titration was required to achieve good light transmission through the gels. It was also evident that the amount of crosslinking required to gelate the collagen solution was reduced as the level of fibrillogenesis progressed. Thus, it was necessary to establish a balance between the solution pH and crosslinker concentration. Implantation of the collagen constructs into partial depth intra-stromal pockets in rabbits was followed up for 6 months, and demonstrated favourable biocompatibility. This showed that gels which had lower levels of both fibrillogenesis and crosslinking were degraded more readily by the host tissue. The collagen gels described here are mass-production friendly, and have promise as potential functional stromal equivalents for use in stromal grafting, or in constructing full thickness artificial corneas.

1. Introduction

The cornea is the tough and precisely curved transparent window at the front of the eye which, aided by the crystalline lens in the eye's interior, focuses light onto the retina. The bulk of the cornea is made up of a collagen-rich stroma, bound either side by epithelial and endothelial cell layers. The corneal stroma possesses the mechanical strength needed to form the anterior outer coat of the eye, whilst still maintaining the high degree of transparency necessary for light transmission. Light transmission through the cornea is a result of a tissue-specific arrangement of uniformly thin collagen fibrils that measure approximately 30 nm in diameter in the hydrated state in man [1] (somewhat smaller when the tissue is fixed, dehydrated, embedded and observed in the electron microscope [2]). Collagen fibrils in the corneal stroma are arranged into a stacked array of about 250 layers or lamellae [3], which are thinner and more interwoven in the anterior cornea [4]. In humans the corneal stroma is approximately 500 μm thick [5], with commonly used experimental animal models having stromal thicknesses which vary from approximately 65–90 μm in mice (depending on the strain) [6,7], 450 μm in rabbit [8], and 800 μm in cow [9].

Theories of corneal transparency hold that the regular short-range spatial order in the collagen fibril array within each lamella allows for light transmission via interference effects [10–12]. This is evidenced by the opaque nature of the adjacent sclera – the white

* Corresponding author. Department of Ophthalmology, Osaka University Medical School, Suita, Osaka, Japan.
E-mail address: knishida@ophthal.med.osaka-u.ac.jp (K. Nishida).
[1] Equal contribution to this work.

0142-9612/$ – see front matter Crown Copyright © 2010 Published by Elsevier Ltd. All rights reserved.
doi:10.1016/j.biomaterials.2010.08.042

of the eye – which like cornea is a collagen-rich connective tissue, but with a less uniform fibril architecture. The characteristic collagen fibril arrangement in the cornea is believed to be maintained by the influence of different molecular subtypes within collagen fibrils [13], and by proteoglycan macromolecules which associate with the collagen and occupy the extrafibrillar space [9,14,15]. Collagen directionality in the plane of the cornea is also an important feature of the tissue, and is believed to affect the cornea's biomechanical stability [16]. Light scattering by cells called keratocytes, which occupy the stroma and which are interspersed between the collagen fibrils and lamellae, is minimized by the high concentration of water soluble proteins called transkeletolase and aldehyde dehydrogenase type I within the cells [17,18].

The arrangement of collagen has a key role in tissue function and the formation of a transparent and mechanically robust corneal stroma. However, the inherent complexity of the tissue's architecture has meant that it is difficult to produce effective constructs that mimic corneal structure and function [19,20]. For example, collagen fibril diameter, fibril spacing and fibrillar alignment, crucial for the mechanical and optical properties of the corneal stroma, would need precise regulation in order to successfully engineer a biomaterial that effectively resembles the stromal matrix and which has potential applications as a tissue substitute. At present this is difficult to achieve at the scale required for usable tissue construct size, although progress is being made [21].

As an alternative to generating a precisely ordered fibrillar structure, collagen gels have been investigated as possible corneal replacements. Over the last decade, scaffolds constructed from long collagen type I fibrils have been studied for use as potential stromal constructs [22–25]. Though highly biocompatible, these collagen

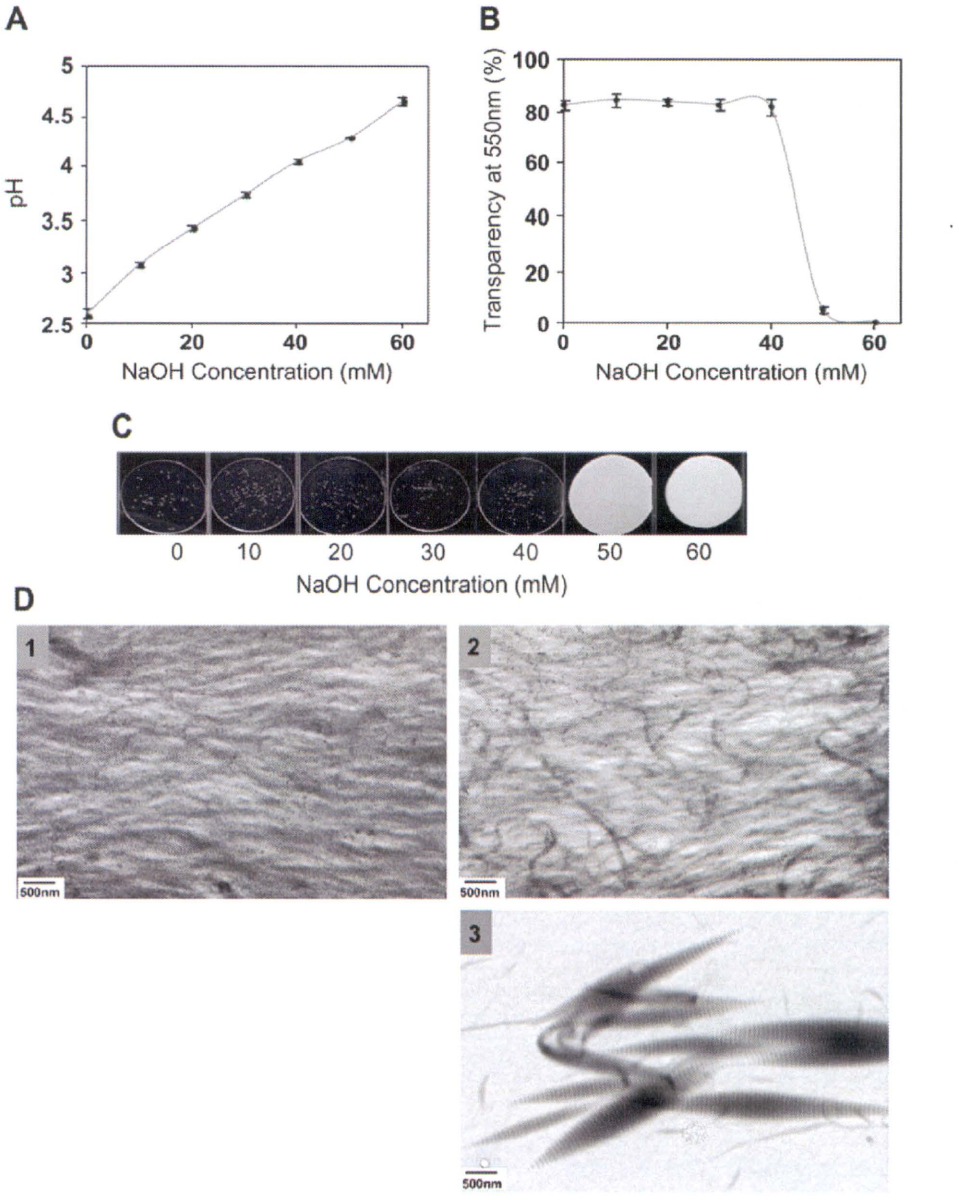

Fig. 1. Deacidification of a 10% (w/w) collagen solution through the addition of NaOH. (A) pH changes in the collagen solution upon NaOH addition. (B) Transparency changes in the collagen solution upon NaOH addition. (C) Photo image. (D) TEM images of collagen solutions using (1) 20 mM, (2) 40 mM, and (3) 60 mM of NaOH. The thickness of specimens in (A), (B) and (C) is 500 nm.

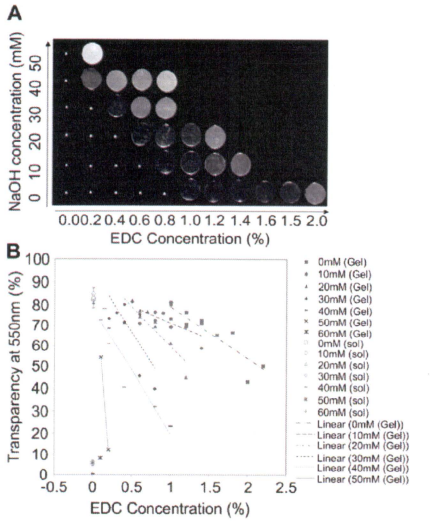

Fig. 2. Collagen gels formed by adding EDC/NHS crosslinking agents to deacidified collagen solutions. (A) Photo image and (B) transparency of collagen gels made using different NaOH and crosslinker levels. All samples are 500 μm thick, with a final collagen concentration of 10% (w/w), and a 2:1 weight ratio of EDC and NHS crosslinking agents. In (A) * denotes inadequate gel formation.

gels are often mechanically instable and have reduced transparency. The effect of including crosslinking agents or glycosaminoglycans on the mechanical and structural characteristics of collagen constructs has also been examined [26–29], although we are still a long way off being able to fabricate and modulate a fibrillar arrangement using proteoglycan additions. Little attention, however, has been paid to the structural and mechanical properties of type I collagen constructs formed at lower pH levels, the focus of this paper.

At high concentrations, type I collagen molecules will self assemble into a liquid crystalline array. By altering the conditions under which the construct is formed, it may be possible to produce a biocompatible tissue substitute which can accurately reproduce the structural and functional capabilities, though not the natural physiologic microanatomy, of the corneal stroma. In the current study we utilized atelocollagen, a telopeptide-free collagen molecule solution formed into a gel. To crosslink the gels, we applied a mixture of ethyl (dimethylaminopropyl) carbodiimide (EDC) and *N*-hydroxysuccimide (NHS) because these agents exhibit better biocompatibility and less toxicity than other crosslinkers such as glutaraldehyde. By manipulating the molecular assembly of highly concentrated atelocollagen solutions and optimizing the chemical environment, we were recently able to produce a transparent and mechanically stable crosslinked collagen gel using flow manipulation [30], which was well tolerated and incorporated into rabbit corneal stromas. The current study reports the transparency, ultrastructural directionality, bi-axial mechanical behavior and long term tolerance and integration into host tissue.

2. Materials and methods

2.1. Collagen solution and gel preparation

Acid freeze-dried type I porcine atelocollagen powder containing 5% type III collagen (Nippon Meat Packers) was dissolved at 4 °C in an HCl aqueous solution (pH 3.0) using a syringe mixing technique [31–34]. Centrifugation overnight at 3500 rpm was used to remove any air bubbles that were present. The pH of the collagen solution was then tuned to 3.5 by the addition, in an ice-water bath, of a NaOH 1.0 M aqueous solution using the same syringe mixing method. To create the gels, collagen solutions were mixed with a crosslinking solution of EDC/NHS (EDC:NHS = 2:1) until a homogeneous mixture was achieved. The final concentration of collagen was adjusted to 10% wet weight and that of EDC to 0.6% wet weight.

2.2. Collagen fibril alignment within the gel

Within 3 min of mixing the crosslinking agent with the collagen solution, 0.5 ml of the mixture was spread onto a glass slide in a 30 mm oval configuration. An elastic film was then placed on top, and a roller was used to spread the mixture in a unilateral direction. Silicon rubber spacers placed between the glass slide and the elastic film regulated the thickness of the gel to 500 μm. Incubation for 12 h at 20 °C and for 12 h at 37 °C was followed by PBS washing at 4 °C.

2.3. Transparency testing

500 μm thick collagen gels, or samples of non-crosslinked atelocollagen, were placed between two glass slides, separated by 500 μm thick silicon rubber spacers and held together with Parafilm. At room temperature, the transparency of the gels was measured using UV/vis-spectroscopy (UV-2550/2450, SHIMAZU, Japan) for narrow spectral regions centered at 400, 450, 500, 550, 600, 650, and 700 nm.

2.4. Mechanical testing

The mechanical characteristics of the collagen gels were tested in directions parallel to and at right angles to the direction of flow manipulation. The 500 μm thick gels were formed into dumb-bell shapes to prevent rupture at the point of attachment and to provide a larger area on which to attach the apparatus. A Universal Testing Instrument (EZ Test, SHIMADZU, Japan) was used at a rate of 100 mm/min to measure a rectangular region of the gels approximately 10 mm by 3 mm in size. The stress was measured as a function of strain, and by analyzing the linear region of the resulting stress-strain curve the elastic modulus of the constructs was calculated.

2.5. In vivo implantation

Three circular collagen gels with unilateral collagen orientation, 8 mm in diameter and approximately 135 μm thick were implanted into mid-depth stromal pockets of six male New Zealand White rabbits (2.0–3.5 kg; Kitayama Labs Co., Nagano, Japan). To achieve this, the rabbits were anesthetized intramuscularly with a mixture of ketamine hydrochloride (60 mg/kg; Sankyo, Tokyo, Japan) and xylazine (10 mg/kg; Bayer, Munich, Germany). A 6 mm-long circumferential incision was then made at the limbus and a stromal pocket created throughout the cornea at midstromal depth after which a rolled up gel was inserted and unfolded *in situ*. The following gels were implanted: 30 mM of NaOH with 0.8% EDC concentration, 30 mM of NaOH with 0.4% EDC concentration, and 10 mM of NaOH with 0.8% EDC concentration. The effect of the three different combinations of NaOH and crosslinker was assessed by histology and/or transmission electron microscopy at 1 and 6 months post-operative time points. An ultrasonic pachymeter used to measure the thickness of the cornea at regular intervals during the post-implantation period. Post-operatively, saline containing antibiotic medication was administered daily. All experimental procedures conformed to the ARVO (Association for Research in Vision and Ophthalmology) Statement for the Use of Animals in Ophthalmic and Vision Research and to local ethical rules.

2.6. Transmission electron microscopy

In vitro constructs and corneas which had been implanted with constructs up to the 6 month time point underwent the same processing routine, which involved immersion in a primary fixative containing 2.5% glutaraldehyde, 2% paraformaldehyde, and 1 M sodium cacodylate buffer for 3 h. En-bloc staining in 2% osmium textroxide and in 0.5% uranyl acetate for 1 h at room temperature was then followed by dehydration through a series of graded alcohols and propylene oxide, before embedding in Araldite resin. A Leica EM.UC6 ultramicrotome (Leica, Tokyo) was used to cut ultrathin sections (approx. 90 nm thick as assessed by the silver/gold interference colour), which were then mounted onto uncoated 200-square mesh copper grids. To analyze non-crosslinked collagen, a droplet of collagen in solution was wiped across the surface of a carbon-coated copper mesh grid. All grids were sequentially stained at room temperature, face down, on 25 μm droplets of 2% uranyl acetate, followed by 1% phosphotungstic acid with washes in between and after. A

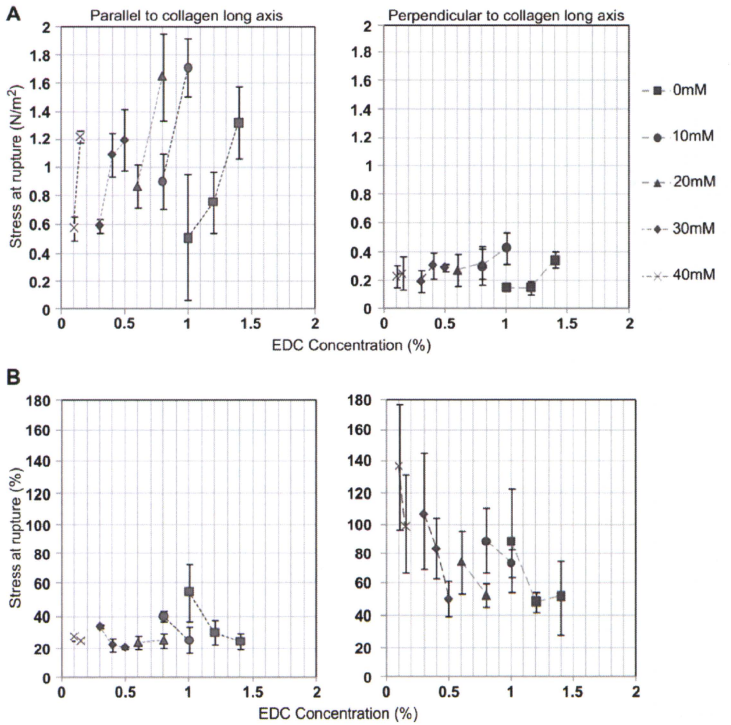

Fig. 3. Mechanical properties of collagen gels: (A) Stress measured in a direction parallel to and perpendicular to collagen alignment. (B) Strain measured in a direction parallel to and perpendicular to collagen alignment. Samples had transparency levels above 70%. All samples were 500 μm thick, with a final collagen concentration of 10% (w/w), and a 2:1 weight ratio of EDC and NHS crosslinking agents.

Hitachi H-7600 TEM (Hitachi, Japan) with a digital camera was used to image samples.

3. Results

Increasing the amount of NaOH used in the formation of the collagen solutions increased their pH, but reduced their transparency (Fig. 1). The effect on transparency was not linear however, with a clear step-change seen at NaOH levels above 40 mM. Below 40 mM of NaOH, transparency remained approximately constant at above 80% light transmission. An increase in NaOH concentration from 40 mM to 50 mM increased the pH of the solution from 4.05 to 4.29 – a relatively minor change – however, the effect on transparency was a profound, dropping from 82% to 6% light transmission (Fig. 1B). By 60 mM NaOH – the highest used in these experiments – pH was 4.66 and transparency measured less than 1%. At NaOH concentrations of 40 mM and below the collagen gels showed some directionality in flow manipulation. However, it was only at 60 mM of NaOH that any fibrils were formed that possessed the characteristic D-banding, and these resembled large tactoids reported by others [35,36] (Fig. 1D).

By crosslinking the collagen solution, a gel could be produced. It is clear from Fig. 2 that as NaOH levels increase, transparency of the gel decreases similar to the effect on collagen solutions shown in Fig. 1. Increasing the levels of crosslinking also reduces the transparency of the gel. Consequently, as the amount of NaOH was increased in the gels, the amount of crosslinking needed to be reduced accordingly in order to keep desirable levels of transparency (Fig. 2). Crosslinking the collagen solutions, as expected, had the effect of improving their mechanical stability, increasing their tensile strength and decreasing the strain at rupture (Fig. 3). All gels tested for mechanical stability had transparency levels above 70%. Concurrent with the transparency data presented in Fig. 2, at higher NaOH levels less crosslinking was required to produce a mechanically stable gel. For example, similar stress levels at rupture were seen in gels made with 30 mM NaOH and 0.5% EDC concentration, as well as in gels made with 40 mM NaOH but which had received only 0.15% EDC. The improvement in mechanical

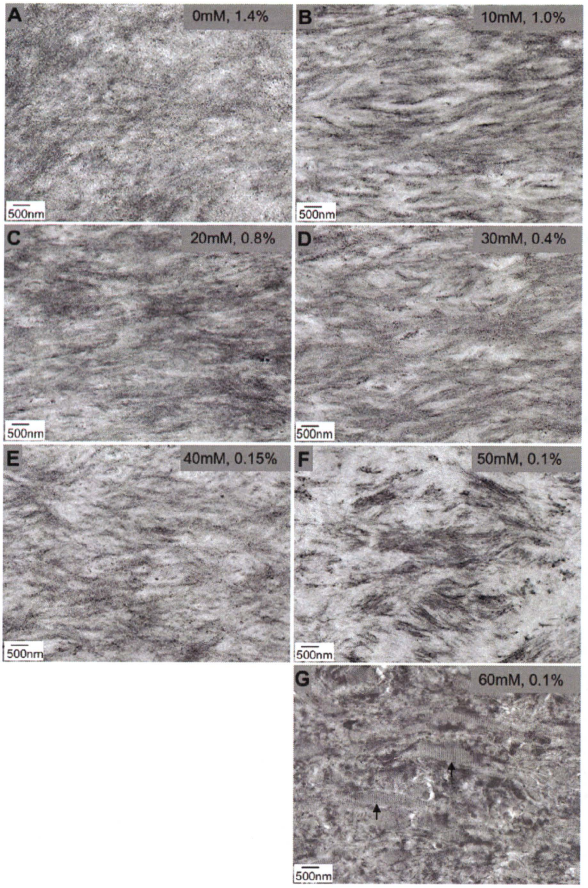

Fig. 4. TEM images of collagen gels at ×3500 magnification. All samples were 500 μm thick. Gel conditions are (A) 0 mM NaOH, 1.4% EDC/NHS (B) 10 mM NaOH, 1.0% EDC/NHS (C) 20 mM NaOH, 0.8% EDC/NHS (D) 30 mM NaOH, 0.4% EDC/NHS (E) 40 mM NaOH, 0.15% EDC/NHS (F) 50 mM NaOH, 0.1% EDC/NHS (G) 60 mM NaOH, 0.1% EDC/NHS. Black arrows in micrograph indicate tactoids.

strength that accompanied crosslinker addition responded to smaller rises in crosslinker percentage as NaOH levels were increased. For example, 0 mM NaOH gels showed a close-to-doubling in tensile strength (from 0.75 N/m^2 to 1.32 N/m^2) when the crosslinker concentration was increased by 0.2%. However, in 40 mM NaOH gels, a similar magnitude rise in tensile strength (from 0.57 N/m^2 to 1.22 N/m^2) was achieved through just a 0.05% increase in crosslinker concentration (Fig. 3). This data also implies that a uniaxial alignment of collagen during gel formation using the flow manipulation approach influences the mechanical behavior of the constructs. For example, the tensile strength of gels tested was approximately three fold higher in a direction parallel to the axis of the collagen than in the perpendicular direction. Strain levels, moreover, were approximately doubled when tensile loading was applied in a direction at right angles to the collagen long axis, than when loaded along the collagen axis. Using increased levels of crosslinker reduced the level of strain at rupture, whilst higher levels of NaOH caused greater levels of strain (Fig. 3).

Transmission electron micrographs of the gels were taken at each different NaOH condition used: 0 mM, 10 mM, 20 mM, 30 mM,

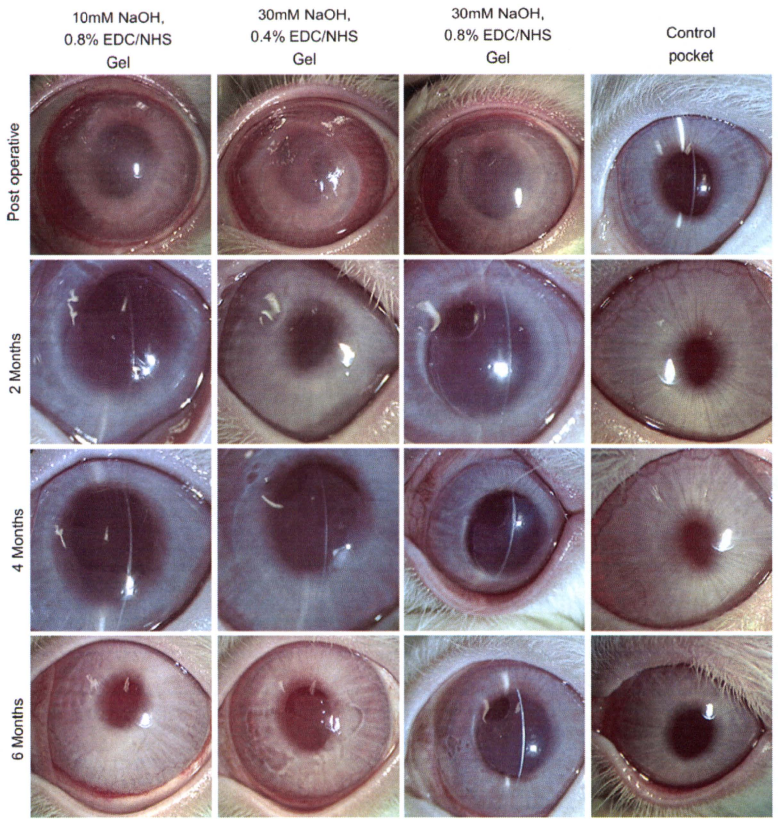

Fig. 5. Six month implantation of collagen gels into rabbit intra-stromal pockets. Collagen gel dimensions were 8 mm in diameter and 100–200 μm in thickness.

40 mM, 50 mM and 60 mM. This revealed that as NaOH levels increased there was a progressive condensation of the collagen within the gel into progressively longer filamentous structures (Fig. 4). At pH 2.6 (i.e. with 0 mM of NaOH) the collagen was present in the gel as a loose matrix with little clear ultrastructure. Increasing the pH to 3.08 using 10 mM of NaOH resulted in the formation of aggregates or bundles of collagen with a clear directionality because of the flow manipulation used in the gel manufacture and which is manifest in preferential strength along the axis of the collagen. Repeated addition of 10 mM NaOH increased the pH of the gels to 3.42, 3.73 and 4.05, respectively. This resulted in the formation of increased levels of aggregation (Fig. 4), and at a pH of 4.29 using 50 mM of NaOH the collagen was organized into more compact bundled structures than was the case for the 30 mM or 40 mM NaOH gels (Fig. 4). More mature fibrils, demonstrating a characteristic D-periodicity banding pattern, could only be seen in gels made with 60 mM of NaOH, as was the case for the collagen in solution (Fig. 1D).

Collagen gels made with different NaOH/crosslinker combinations are all well tolerated when implanted into mid-depth rabbit corneal intra-stromal pockets with no sign of inflammation or rejection. The three different gel types all show good biocompatibility and transparency up to 6 months post-operatively (Fig. 5). In the immediate post-operative period the thickness of the operated corneas measured by ultrasonic pachymetry (Fig. 6) is significantly increased due to a combination of the addition of extra material in the stroma and to the intrusive nature of the surgical procedure itself – i.e. the sham operated pocket-only cornea is approximately 150 μm thicker after surgery indicating that the stroma does not immediately revert to normal. One week after surgery, however, the control surgical cornea has returned to near normal thickness, whereas the implanted corneas all remain significantly thicker than

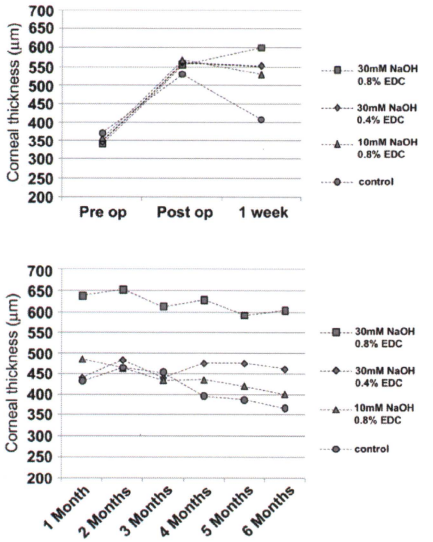

Fig. 6. Rabbit corneal thickness measurements following implantation of collagen gels into midstromal rabbit pockets. Collagen gel dimensions were approximately 8 mm in diameter.

pre-implant values (Fig. 6A). A subsequent reduction in corneal thickness of the construct-implanted corneas over the following several months suggests that there may be some incorporation, remodeling or digestion of the gels by the host tissue. It was notable from the thickness measurements, however, that the 30 mM NaOH gel crosslinked with 0.8% EDC appears to have resisted the digestion more than the other gel types over the implantation period.

The incorporation, remodeling or digestion of implanted gels was confirmed by histological analysis (Fig. 7). In all cases, the 30 mM NaOH, 0.8% EDC/NHS gel was prominent in the host tissue, even 6 months after implantation. Moreover, some oedema seems to have occurred in the anterior region stroma above this implant by this time point possibly due to a restriction in the diffusion of metabolites through the stroma. The 30 mM NaOH, 0.4% EDC/NHS gel is still evident in the stroma 6 months post-implantation, but no anterior stromal oedema seems to have occurred in this case. The 10 mM NaOH gel was the least retained of the gels tested, with minimal gel remaining 1 month after implantation.

TEM analysis of the implanted gels *in situ* showed that the invasion of host cells into the gels was often accompanied by remodeling or digestion of the gels (Fig. 8). Despite the gels being crosslinked during their fabrication, their morphological appearance changed after prolonged placement within the host tissue. A relatively high level of collagen fibril formation could be seen in the 30 mM/0.8% gel after 6 months of implantation compared to the 1 month time point, suggestive of a progression in fibrillogenesis during the implantation period. Similar to the results seen in Fig. 4, the morphological properties of the gels *in situ* does vary depending on the ratio and amounts of NaOH and crosslinkers used during their production – with lower NaOH and crosslinker levels producing a gel with a less well defined matrix of more loosely associated collagen filaments. In agreement with histological observations (Fig. 7), the 10 mM NaOH, 0.8% EDC/NHS gel was not observed in the stroma at the time of sacrifice. Only at 1 month post-implantation could any remnants of this gel be found under TEM analysis (Fig. 8). Cellular infiltration was also more prevalent in the 10 mM/0.8%, and 30 mM/0.4% gels.

4. Discussion

The data presented here shows the critical importance if producing a suitable chemical environment if we are to fabricate a functional and implantable gel-like biomimetic collagen construct for use in corneal surgery. The changes in light transmission in the collagen solutions with varying pH demonstrate that a critical point is reached just above pH 4.0, after which the pH has a highly detrimental effect on the transparency of the collagen solutions. A similar pattern of reduced light transmission with higher NaOH levels was seen for the crosslinked collagen gels, but in this case the situation was less straightforward because at identical pH levels, light transmission was differently affected depending on the amount of chemical crosslinker used. Not inducing sufficient crosslinking, however, would result in a mechanically unstable gel, thus it was necessary to find a balance between these two factors in order to produce a robust, flexible and usable transparent gel. Based on these initial experiments, gels judged to be potentially suitable for grafting into living tissue were chosen as 30 mM NaOH with 0.8% EDC, 30 mM NaOH with 0.4% EDC, and 10 mM NaOH with 0.8% EDC.

Crosslinking, as expected, enhanced the mechanical strength of the collagen gels – improving tensile strength in a direction parallel to collagen alignment, and improving the elastic properties of the gels in a perpendicular direction. Interestingly, the elastic properties of the gels parallel to the flow direction were found to be similar to those of human corneal tissue (3.81 ± 0.40 N/mm^2 in tensile strength [37], 3–13 N/mm^2 in Young's modulus [38]).

Constructs formed under increasingly basic conditions demonstrated greater stress and strain levels at rupture in both the plane parallel to, and the plane perpendicular to, the collagen axis. The observation that the stress–strain relationship is a function of pH has been reported in numerous other studies involved collagen hydrogels [39,40]. In these published studies, the length and diameter of the forming collagen fibrils, along with their organization, had a dramatic impact on the mechanical properties of the constructs. For example, Parry has shown that increased levels of small diameter collagen fibrils protect tendon tissue structure from plastic deformation [41]. Roeder and associates have also reported that an increased pH had the effect of increasing fibril length and decreasing fibril diameter, which in turn improved the mechanical properties of the collagen matrices [40]. It has been suggested that fibril length has a greater influence on the viscoelastic properties than does fibril diameter [40,41]. In particular the longitudinal fusion of fibril subunits increases the resistance to high strain level deformation. The lateral fusion of fibril subunits also has an impact on mechanical properties, but this was found to be specific to low strain level deformation resistance [39].

TEM images of the gels produced here show that the diameter of the condensing collagen structures appears to decrease as pH increases. Research by others which has focused on the later stages of fibril assembly at higher pH levels, have also observed similar results [39,42]. In our micrographs a range of subfibrillar intermediates could be identified - from a largely disorganized matrix of collagen molecules, through intermittent molecular aggregations,

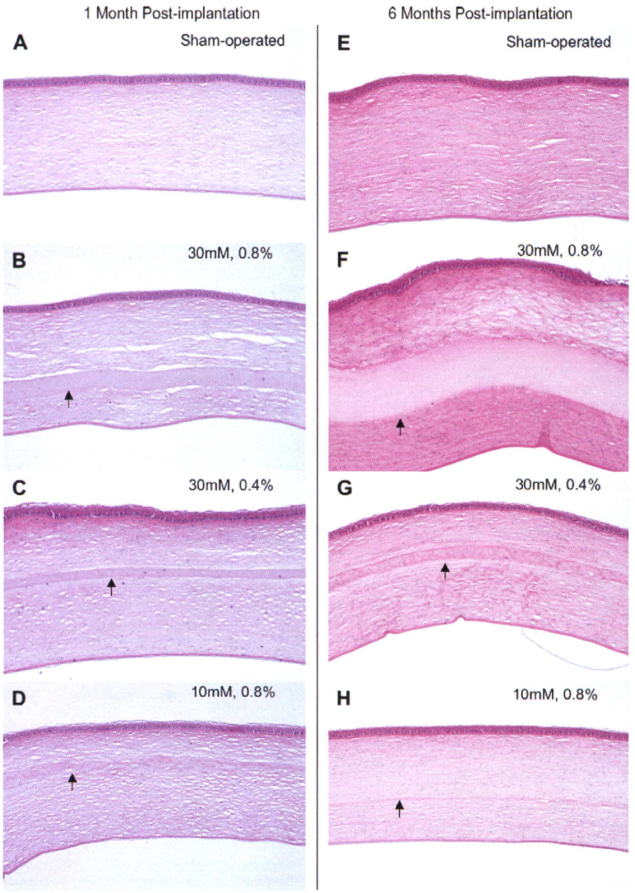

Fig. 7. 1 and 6 months post-implantation. Rabbit corneal cross sections with various collagen gels implanted into an intra-stromal pocket. Black arrows indicate the posterior surface of the implant. A: Control, B: 30 mM NaOH 0.8% EDC/NHS, C: 30 mM NaOH 0.4% EDC/NHS, D: 10 mM NaOH 0.8% EDC/NHS 1 month post-implantation. E: Control, F: 30 mM NaOH 0.8% EDC/NHS, G: 30 mM NaOH 0.4% EDC/NHS, H: 10 mM NaOH 0.8% EDC/NHS 6 months post-implantation.

to the formation of progressively condensing filamentous structures. At the lower pH levels, the condensing collagen filaments resembled the pathologically unraveling collagen fibrils that are found in necrotizing scleritis [43]. Higher pH levels resulted in the formation of tactoid-like structures [35] that possessed D-periodic banding. Similar results have been observed by other investigators, however, no fully mature collagen fibrils were observed in their studies [44]. *In vitro*, mature collagen fibrils that possess the characteristic D-banded periodicity occur when fibrillogenesis is carried out under greater pH levels [32,45–47].

The TEM images show that at NaOH levels above 40 mM, the filament structures within the gels demonstrate a high degree of compaction, and have associated into groups. Subsequently, the matrix of the gel appears considerably more heterogeneous. It may be that a fairly uniform refractive index within the gels was responsible for low levels of light scattering in the construct and the resultant good transparency. Loss of this ultrastructural uniformity might be responsible for the subsequent reduction in transparency.

Previous *in vivo* studies have shown that crosslinked collagen gels possess satisfactory biocompatibility for integration into

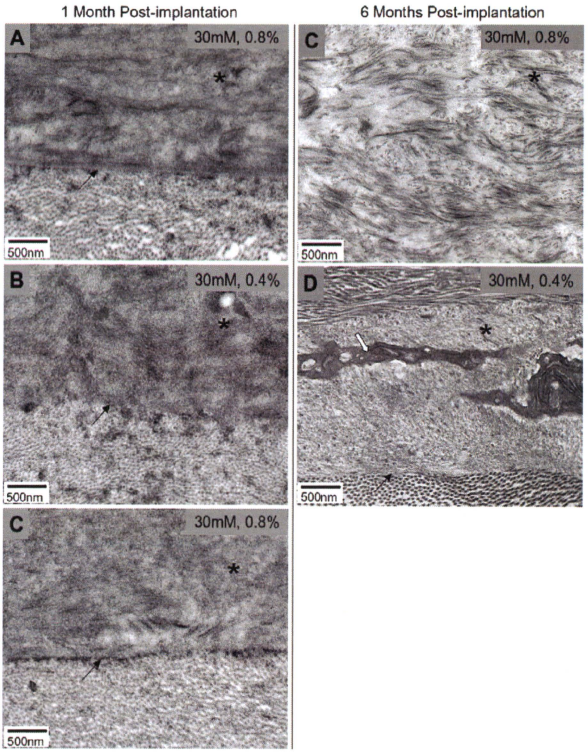

Fig. 8. 1 and 6 months post-implantation. TEM images at ×6000 magnification, of rabbit corneal stroma with various collagen gels implanted into an intra-stromal pocket. Before implantation the gel had a final collagen concentration of 10% (w/w).Asterisks indicates collagen gel implant. Black arrow indicates boundary between host stroma and gel implant. White arrow indicates invading host stromal cell. A: 30 mM NaOH 0.8% EDC/NHS, B: 30 mM NaOH 0.4% EDC/NHS at 1 month post-implantation. C: 30 mM NaOH 0.8% EDC/NHS, D: 30 mM NaOH 0.4% EDC/NHS at 6 months post-implantation.10 mM NaOH, 0.8% EDC/NHS gel was no longer present in the stroma at 6 months post-implantation.

stromal tissue and re-growth of host epithelial cells [32–34,48]. Our findings support the potential use of collagen-based constructs for clinical use as corneal stromal implants. The enhanced stability of the 30 mM NaOH, 0.8% EDC crosslinked gel within the intra-stromal pocket suggests that higher crosslinker levels, when coupled with greater levels of collagen fibrillogenesis, delay the digestion or degradation of the construct. However, the detrimental effect that these levels have on transparency of the gel must be taken into consideration. In addition, oedma in the anterior stroma suggests that the most stable gel (30 mM of NaOH, 0.8% EDC/NHS) may act as a barrier, preventing the endothelial pump from properly regulating anterior stromal hydration.

5. Conclusions

It is clear that within our constructs the assembly of type I collagen molecules can be manipulated over a wide pH range. In addition, even minor changes in the environmental conditions of the gels (such as pH), dramatically affects the optical and mechanical properties of the constructs. It was therefore necessary to establish a balance between the solution pH and crosslinker concentration. Nevertheless, whilst *in vitro* analysis can highlight the fundamental processes that govern fibrillogenesis, we must be careful to observe the limitations of any comparisons made to natural collagen assembly, as the complex arrangement of keratocytes and ECM macromolecules creates a unique and influential environment that cannot currently be replicated *in vitro*. *In vivo* implantation of the hydrogels into intra-stromal pockets demonstrated favourable biocompatibility, and highlighted the effect of higher levels of both fibrillogenesis and crosslinking on increased long term survival of the gels. Further work will be aimed at enhancing the optical and mechanical properties of the gels, and improving their long term *in vivo* characteristics through the addition of other ECM molecules. Presently, the optically transparent crosslinked collagen gels used in this study provide a basis for the future production of more complex biomimetic stromal

constructs utilizing orthogonally stacked layers of aligned collagen. The gels used in this study have potential clinical use as drug carriers, as protective membranes for corneal surface damage, and stromal implantation for tissue replacement and regeneration.

Acknowledgements

We thank EPSRC (UK) and Global COE (Japan) for supporting this study. This work was supported in part by grants from the United Kingdom Engineering and Physical Sciences Research Council (Grant no. EP/F034970/1 to AJQ), the Grants-in-Aid for Scientific Research from the Ministry of Health Labor and Welfare, and from the Ministry of Education, Culture, Sports, Science, and Technology in Japan, and by the Tohoku University Global COE for conquest of Signal Transduction Disease with "Network Medicine". The authors confirm that there are no known conflicts of interest associated with this publication and there has been no significant financial support for this work that could have influenced its outcome.

References

[1] Meek KM, Leonard DW. Ultrastructure of the corneal stroma: a comparative study. Biophys J 1993;64:273–80.
[2] Quantock AJ, Meek KM, Fullwood NJ, Zabel RW. Scheie's syndrome: the architecture of corneal collagen and distribution of corneal proteoglycans. Can J Ophthalmol 1993;28:266–72.
[3] Hogan MJ, Alvarado JA, Weddel JE. Histology of the Human Eye. Philadelphia: WB Saunders; 1971. pp. 55–111, 183–201.
[4] Komai Y, Ushiki T. The three-dimensional organization of collagen fibrils in the human cornea and sclera. Invest Ophthalmol Vis Sci 1991;32:2244–58.
[5] Ivarsen A, Fledelius W, Hjortdal JO. Three-year changes in epithelial and stromal thickness after PRK or LASIK for high myopia. Invest Ophthalmol Vis Sci 2009;50:2061–6.
[6] Hayashida Y, Akama TO, Beecher N, Lewis P, Young RD, Meek KM, et al. Matrix morphogenesis in cornea is mediated by the modification of keratan sulfate by GlcNAc 6-O-sulfotransferase. Proc Natl Acad Sci U S A 2006;103:13333–8.
[7] Henriksson JT, McDermott AM, Bergmanson JPG. Dimensions and morphology of the cornea in three strains of mice. Invest Ophthalmol Vis Sci 2009;50:3648–54.
[8] Müller L, Pels E, Vrensen G. The specific architecture of the anterior stroma accounts for maintenance of corneal curvature. Br J Ophthalmol 2001;85:437–43.
[9] Quantock AJ, Young RD, Tomoya AO. Structural and biochemical aspects of keratan sulphate in the cornea. Cell Mol Life Sci 2010;67:891–906.
[10] Maurice DM. The structure and transparency of the corneal stroma. J Physiol 1957;136:263–86.
[11] Hart RW, Farrell RA. Light scattering in the cornea. J Opt Soc Am 1969;59:766–74.
[12] Benedek GB. Theory and transparency of the eye. Appl Opt 1971;10:459–73.
[13] Birk DE, Fitch JF, Babiarz JP, Doane KJ, Linsenmayer TF. Collagen fibrillogenesis in vitro: interaction of types I and V collagen regulates fibril diameter. J Cell Sci 1990;95:649–57.
[14] Zhang G, Chen S, Goldoni S, Calder BW, Simpson HC, Owens RT, et al. Genetic evidence for the coordinated regulation of collagen fibrillogenesis in the cornea by decorin and biglycan. J Biol Chem 2009;284:8888–97.
[15] Lewis PN, Pinali C, Young RD, Meek KM, Quantock AJ, Knupp C. Structural interactions between collagen and proteoglycans are elucidated by three-dimensional electron tomography of bovine cornea. Structure 2010;18:239–45.
[16] Meek KM, Boote C. The use of X-ray scattering techniques to quantify the orientation and distribution of collagen in the corneal stroma. Prog Retin Eye Res 2009;28(5):369–92.
[17] Jester JV, Møller-Pedersen T, Huang J, Sax CM, Kays WT, Cavangh HD, et al. The cellular basis of corneal transparency: evidence for 'corneal crystallins'. J Cell Sci 1999;112:613–22.
[18] Jester JV. Corneal crystallins and the development of cellular transparency. Semin Cell Dev Biol 2008;19:82–93.
[19] Hu X, Lui W, Cui L, Wang M, Cao Y. Tissue engineering of nearly transparent corneal stroma. Tissue Eng 2005;11(11–12):1710–7.
[20] Orwin EJ, Borene ML, Hubel A. Biomechanical and optical characteristics of a corneal stromal equivalent. J Biomech Eng 2003;125:439–44.
[21] Ruberti JW, Zieske JD. Prelude to corneal tissue engineering – gaining control of collagen organization. Prog Retin Eye Res 2008;27(5):549–77.
[22] Germain L, Auger FA, Grandbois E, Guignard R, Giasson M, Boisjoly H, et al. Reconstructed human cornea produced in vitro by tissue engineering. Pathobiology 1999;67(3):140–7. LOEX.
[23] Griffith M, Hakim M, Shimmura S, Watsky M, Li F, Carlsson D, et al. Artificial human corneas: scaffolds for transplantation and host regeneration. Cornea 2002;21(Suppl. 2):S54–61.
[24] Schneider AI, Maier-Reif K, Graeve T. Constructing an in vitro cornea from cultures of the three specific corneal cell types. In Vitro Cell Dev Biol Anim 1999;35(9):515–26.
[25] Tegtmeyer S, Papantoniou I, Muller-Goymann CC. Reconstruction of an in vitro cornea and its use for drug permeation studies from different formulations containing pilocarpine hydrochloride. Eur J Pharm Sci 2001;51(2):119–25.
[26] Chen CS, Yannas IV, Spector M. Pore strain behaviour of collagen-glycosaminoglycan analogues of extracellular matrix. Biomaterials 1995;16(10):777–83.
[27] Matsuda K, Suzuki S, Isshiki N, Yoshioka K, Okada T, Ikada Y. Influence of glycosaminoglycans on the collagen sponge component of a bilayer artificial skin. Biomaterials 1990;11(5):351–5.
[28] Osborne CS, Barbenel JC, Smith D, Savakis M, Grant MH. Investigation into the tensile properties of collagen/chondroitin-6-sulphate gels: the effect of crosslinking agents and diamines. Med Biol Eng Comput 1998;36(1):129–34.
[29] Yannas IV, Burke JF. Design of an artificial skin. I. Basic design principles. J Biomed Mater Res 1980;14(1):65–81.
[30] Tanaka Y, Kubota A, Matsusaki M, Duncan T, Hatakeyama Y, Fukuyama K, et al. Anisotropic mechanical properties in collagen hydrogels induced by uniaxial-flow for ocular applications. J Biomater Sci Polym Ed; 2010. [Epub ahead of print].
[31] Rafat M, Li F, Fagerholm P, Lagali NS, Watsky MA, Munger R, et al. PEG-stabilized carbodiimide crosslinked collagen–chitosan hydrogels for corneal tissue engineering. Biomaterials 2008;29(29):3960–72.
[32] Liu Y, Gan L, Carlsson DJ, Fagerholm P, Lagali N, Watsky MA, et al. A simple, crosslinked collagen tissue substitute for corneal implantation. Invest Ophthalmol Vis Sci 2006;47(5):1869–75.
[33] Liu Y, Griffith M, Watsky MA, Forrester JV, Kuffova L, Grant D, et al. Properties of porcine and recombinant human collagen matrices for optically clear tissue engineering applications. Biomacromolecules 2006;7(6):1819–28.
[34] Liu W, Merrett K, Griffiths M, Fagerholm P, Dravida S, Heyne B, et al. Recombinant human collagen for tissue engineered corneal substitutes. Biomaterials 2008;29(9):1147–58.
[35] Bard JB, Chapman JA. Polymorphism in collagen fibrils precipitated at low pH. Nature 1968;219:1279–80.
[36] Leibovich SJ, Weiss JB. Electron microscope studies of the effects of endo- and exopeptidase digestion on tropocollagen. A novel concept of the role of terminal regions in fibrillogenesis. Biochim Biophys Acta 1970;214(3):445–54.
[37] Zeng Y, Yang J, Huang K, Lee Z, Lee X. A comparison of biomechanical properties between human and porcine cornea. J Biomech 2001;34(4):533–7.
[38] Crabb RA, Chau EP, Evans MC, Barocas VH, Hubel A. Biomechanical and microstructural characteristics of a collagen film-based corneal stroma equivalent. Tissue Eng 2006;12(6):1565–75.
[39] Christiansen DL, Huang EK, Frederick HS. Assembly of type I collagen: fusion of fibril subunits and the influence of fibril diameter on mechanical properties. Matrix Biol 2000;19(5):409–20.
[40] Roeder BA, Kokini K, Sturgis JE, Robinson JP, Voytik-Harbin SL. Tensile mechanical properties of three-dimensional type I collagen extracellular matrices with varied microstructure. J Biomech Eng 2002;124:214–22.
[41] Parry DA. The molecular and fibrillar structure of collagen and its relationship to the mechanical properties of connective tissue. Biophys Chem 1988;29(1–2):195–209.
[42] Trelstad RL, Hayashi K, Gross J. Collagen fibrillogenesis: intermediate aggregates and suprafibrillar order. Proc Natl Acad Sci U S A 1976;73(11):4027–31.
[43] Watson PG, Young RD. Scleral structure, organisation and disease. A review. Exp Eye Res 2004;78(3):609–23.
[44] Harris JR, Reiber A. Influence of saline and pH on collagen type I fibrillogenesis in vitro: fibril polymorphism and colloidal gold labelling. Micron 2007;38(5):513–21.
[45] Cisneros DA, Hung C, Franz CM, Muller DJ. Observing growth steps of collagen self-assembly by time-lapse high-resolution atomic force microscopy. J Struct Biol 2006;154(3):232–45.
[46] Gelman RA, Poppke DC, Piez KA. Collagen fibril formation in vitro. The role of the nonhelical terminal regions. J Biol Chem 1979;254(22):11741–5.
[47] Graham HK, Holmes DF, Watson RB, Kadler KE. Identification of collagen fibril fusion during vertebrate tendon morphogenesis. The process relies on unipolar fibrils and is regulated by collagen-proteoglycan interaction. J Mol Biol 2000;295(4):891–902.
[48] Merrett K, Liu W, Mitra D, Camm KD, McLaughlin CR, Liu Y, et al. Synthetic neoglycopolymer-recombinant human collagen hybrids as biomimetic crosslinking agents in corneal tissue engineering. Biomaterials 2009;30(29):5403–8.

Original article

A novel method of culturing human oral mucosal epithelial cell sheet using post-mitotic human dermal fibroblast feeder cells and modified keratinocyte culture medium for ocular surface reconstruction

Yoshinori Oie,[1,2] Ryuhei Hayashi,[1] Ryo Takagi,[3] Masayuki Yamato,[3] Hiroshi Takayanagi,[4] Yasuo Tano,[2] Kohji Nishida[1]

[1]Department of Ophthalmology and Visual Science, Tohoku University Graduate School of Medicine, Sendai, Japan
[2]Department of Ophthalmology, Osaka University Medical School, Suita, Japan
[3]Institute of Advanced Biomedical Engineering and Science, Tokyo Women's Medical University, Tokyo, Japan
[4]Translational Research Center, Tohoku University, Sendai, Japan

Correspondence to
Dr Kohji Nishida, Department of Ophthalmology and Visual Science, Tohoku University Graduate School of Medicine, Sendai 980-8574, Japan; knishida@oph.med.tohoku.ac.jp)

Accepted 20 February 2010

ABSTRACT

Background/aims To cultivate human oral mucosal epithelial cell sheets with post-mitotic human dermal fibroblast feeder cells and modified keratinocyte culture medium for ocular surface reconstruction.

Methods Human oral mucosal epithelial cells obtained from three healthy volunteers were cultured with x-ray-treated dermal fibroblasts (fibroblast group) and NIH/3T3 feeder layers (3T3 group) on temperature-responsive culture dishes. Media were supplemented using clinically approved products. Colony-forming efficiency was determined in both groups. Histological and immunohistochemical analyses were performed for cell sheets. Cell viability and purity of cell sheets were evaluated by flow cytometry.

Results Colony-forming efficiency in the fibroblast group was similar to that in the 3T3 group. All cell sheets were well stratified and harvested successfully. The expression patterns of keratin 1, 3/76, 4, 10, 12, 13, 15, ZO-1 and MUC16 were equivalent in both groups. The percentage of p63-positive cells in the fibroblast group (46.1±4.2%) was significantly higher than that in the 3T3 group (30.7±7.6%) (p=0.038, t test). The cell viability and purity were similar between the two groups.

Conclusion This novel culture method using dermal fibroblasts and pharmaceutical agents provides a safe cell processing system without xenogenic feeder cells for ocular surface reconstruction.

Tissue-engineered cell sheets composed of autologous oral mucosal epithelium have been successfully used to reconstruct eyes affected with severe ocular surface disorders.[1 2] However, it is possible that murine fibroblast feeder layers used for human transplantation can transmit murine diseases. In addition, it has been reported that human embryonic stem cells cultured on mouse feeder layers generate immunogenic non-human sialic acid.[3] Therefore, a new processing method that does not use animal-derived material should be developed to avoid this problem.

The use of human adipose tissue-derived and bone marrow-derived mesenchymal stem cells is reported to generate transplantable epithelial cell sheets.[4 5] The risks associated with xenogenic feeder layers can be avoided with these methods. However, the harvesting of adipose tissue or bone marrow is invasive; therefore, an alternative cell source for feeder layers is required for autologous cell therapy.

Dermal fibroblasts have been used as a feeder layer to culture skin keratinocytes,[6 7] and dermal fibroblast can be easily cultured.[8] It is thus thought that dermal fibroblasts can be utilised as an alternative candidate for mesenchymal stem cells or NIH/3T3 cells in culturing oral mucosal epithelial cells.

The supplements in conventional keratinocyte culture medium (KCM) are reagents used for laboratory research. The laboratory-grade supplements in KCM should be replaced with pharmaceutical products approved by the Ministry of Health, Labour and Welfare for clinical application. Modified KCM, which adopted the use of clinical agents as culture supplements, was equally as efficient as conventional KCM in the fabrication of canine, transplantable, stratified epithelial cell sheets.[9]

In particular, we investigated a novel culture method of human oral mucosal epithelial cell sheets using post-mitotic human dermal fibroblast feeder cells and modified KCM with clinically approved supplements.

MATERIALS AND METHODS

Preparation of feeder layers

Human dermal tissues were obtained from three healthy volunteers who provided written informed consent. Human tissue was handled according to the Declaration of Helsinki.

Dermal fibroblasts were cultured using the explant procedure.[8] To prepare feeder layers, human dermal fibroblasts were lethally irradiated with 40 Gly and then trypsinised and seeded onto tissue culture dishes (60 mm diameter; BD Biosciences, San Diego, California, USA) at a density of 5×10^3 cells/cm^2 (fibroblast group). As a positive control, lethally irradiated NIH/3T3 cells were prepared at a density of 2×10^4 cells/cm^2 (3T3 group).

Reverse transcription PCR

Total RNA was obtained from human dermal fibroblasts and NIH/3T3 cells using the GenElute mammalian total RNA kit (Sigma, St Louis, Missouri, USA). Reverse transcription was performed with the SuperScript First-Strand Synthesis System for reverse transcription PCR (Invitrogen, Carlsbad, California, USA), according to the manufacturer's suggested protocol, and cDNA was used as the template for PCR. The reverse transcription PCR thermocycle programme consisted of an initial step at 94°C for 5 min and 30 cycles at 94°C for 30 s and 58°C for 30 s and 72°C

for 30 s (PCR Thermal Cycler MP; Takara, Shiga, Japan). The primer pairs are shown in table 1.

Preparation of modified KCM

Modified KCM was supplemented with clinically approved products. The medium consisted of Dulbecco's modified eagle medium and Ham's F12 medium (Gibco-Invitrogen) at a 3:1 ratio, supplemented with 10% autologous human serum, 5 μg/ml insulin (humulin; Eli Lilly, Indianapolis, Indiana, USA), 2 nM triiodothyronine (thyronamin; Takeda, Osaka, Japan), 0.4 μg/ml hydrocortisone (saxizon; Kowa, Tokyo, Japan), 100 nM L-isoproterenol (proternol; Kowa), 2 mM L-glutamine (Gibco), 10 ng/ml epidermal growth factor (Higeta Shoyu, Chiba, Japan), and 40 μg/ml gentamicin (gentacin; Schering-Plough, Kenilworth, New Jersey, USA).

Oral mucosal epithelial cell culture

Human oral mucosal epithelial tissues were obtained from the same three healthy volunteers, respectively. Therefore, we performed the comparison of the two feeder layers three times in the current study. After the oral cavity of each volunteer was sterilised with topical povidone-iodine, a 3×3 mm specimen of oral mucosal tissue was surgically excised from the interior buccal mucosal epithelium under local anaesthesia with propitocaine. Oral mucosal epithelial cells were collected by removing all epithelial layers after treatment with dispase II (2.4 U/ml; Invitrogen), at 4°C for 4 h. Separated epithelial layers were treated with trypsin-EDTA (Invitrogen), and resuspended cells were plated on temperature-responsive culture inserts (CellSeed, Tokyo, Japan) at an initial cell density of 2.0×10^5 cells/23 mm insert, with feeder cells separated by cell culture inserts.[1] The cells were cultured for 14–17 days.

For colony-forming assays, 3000 or 5000 primary oral mucosal epithelial cells were seeded onto culture dishes (60 mm diameter; BD Biosciences) with irradiated feeder layers. After cultivation for 10–12 days, dishes were fixed and stained with rhodamine B. Colony-forming efficiency was defined as the ratio of the number of colonies to the number of cells inoculated. Colony size was also calculated using scanned photos of stained dishes with Axio Vision LE (Carl Zeiss, Jena, Germany).

Table 1 Primer sequences

Gene	Primer sequence (5′→3′)	Product size (bp)
hPTN	Forward: AGAGGACGTTTCCAACTCAA	551
	Reverse: TATGTTCCACAGGTGACATC	
hEPR	Forward: AGGAGGATGGAGATGCTCTG	498
	Reverse: TCAGACTTGCGGCAACTCTG	
hCC	Forward: TCCTCTCTATCTAGCTCCAG	500
	Reverse: TCCTGACAGGTGGATTTCGA	
hHGF	Forward: GCCTGAAAGATATCCCGACA	523
	Reverse: TTCCATGTTCTTGTCCCACA	
hKGF	Forward: AGGCTCAAGTTGCACCAGGCA	495
	Reverse: TGTGTGTCGCTCAGGGCTGGA	
hShh	Forward: CGGAGCGAGGAAGGGAAAG	262
	Reverse: TTGGGGATAAACTGCTTGTAGGC	
hIGF1a	Forward: ATGCACACCATGTCCTC	390
	Reverse: CATCCTGTAGTTCTTGTTTC	
hN-cad	Forward: ATGCTGACGATCCCAATG	317
	Reverse: GATGTCTACCCTGTTCTCA	
hGAPDH	Forward: ACCACAGTCCATGCCATCAC	452
	Reverse: TCCACCACCCTGTTGCTGTA	
mPTN	Forward: GGACCTCTGCAAGCCAAAAAA	317
	Reverse: GCACTCAGCTCCAAACTGCTTC	
mEPR	Forward: AGCTGCACCGAGAAAGAAGGA	318
	Reverse: AGAAGTGCTCACATCGCAGACC	
mCC	Forward: AGCTCGTGGCTGGAGTGAACTA	343
	Reverse: CCTGCAGCAGCTCCTTTACTGT	
mHGF	Forward: GGTGAAAGCTACAGAGGTCCCA	314
	Reverse: ATGGTATTGCTGGTTCCCCTG	
mKGF	Forward: CGAGGCAGACAGCAGACACGG	504
	Reverse: GTGTCGCTCGGGGCTGGAAC	
mShh	Forward: CCCAAAAAGCTGACCCCTTTAG	335
	Reverse: TCCACTGCTCGACCCTCATAGT	
mIGF1a	Forward: TATGGCTCCAGCATTCGGA	319
	Reverse: GCGGTGATGTGGCATTTTCT	
mN-cad	Forward: AGAGGGATCAAAGCCTGGGACGTAT	360
	Reverse: TCCACCCTGTTCTCAGGGACTTCTC	
mGADPH	Forward: ATCACTGCCACCCAGAAGACTG	325
	Reverse: TGCTGTTGAAGTCGCAGGAGA	

CC, cystatin C; EPR, epiregulin; GAPDH, glyceraldehydes-3-phosphate dehydrogenase; h, human; HGF, hepatocyte growth factor; IGF1a, insulin-like growth factor 1a; KGF, keratinocyte growth factor; m, mouse; N-cad, N-cadherin; PTN, pleiotrophin; Shh, sonic hedgehog.

Cell morphology

Cultured epithelial cells were observed under a phase contrast microscope, and microphotographs were taken at 100-fold magnification (Axiovert40; Carl Zeiss) to examine cell morphological aberrations and deficits.

Sheet recovery test

After examination with phase contrast microscopy, cultured epithelial cells were subjected to incubation at 20°C for 30 min. Then, a donut-shaped support membrane (18 mm outer diameter, 10 mm inner diameter, polyvinylidene difluoride; Millipore, Bedford, Massachusetts, USA) was placed on the epithelial cells. Finally, cells were challenged with harvesting in the presence of support membranes. Harvested epithelial cell sheets were divided into two parts. Half of the cell sheets were subjected to flow cytometry and the other half were subjected to histological analyses.

Cell viability and epithelial cell purity

Cell viability was evaluated with a dye exclusion test. An aliquot of cell suspension was incubated in Dulbecco's modified eagle medium with 7-aminoactinomycin D (BD Biosciences) staining at room temperature for 10 min, and subjected to flow cytometry (FACS Calibur; BD Biosciences).

After trypsin-EDTA treatment, an aliquot of the cell suspension was centrifuged, fixed and permeabilised with the Cytofix/Cytoperm kit (BD Biosciences) according to the manufacturer's protocol. Then, the cell suspension was split into two tubes, and incubated with either a FITC-conjugated anti-pancytokeratin IgG2a antibody (clone Pan1-8; Progen, Heidelberg, Germany) or a FITC-conjugated mouse control IgG2a antibody (Santa Cruz Biotechnology, Santa Cruz, California, USA) at room temperature for 60 min. After being washed twice with PBS, nuclei were stained with 7-aminoactinomycin D and the cells were examined by flow cytometry.

H&E staining and immunofluorescence analyses

The portion of cell sheets to be used in histological analyses was divided into two quadrants. One quadrant was fixed with formalin and embedded in paraffin. H&E staining was performed to observe the morphology and degree of stratification of the cultured epithelial cells. Microphotographs were taken with a light microscope (BZ-9000, Keyence, Osaka, Japan).

The other quadrant of cell sheets was embedded in Tissue-Tek OCT compound (Sakura Seiki, Tokyo, Japan) and processed into